

Versatile New C_3 -Symmetric Tripodal Tetraphosphine Ligands; Structural Flexibility to Stabilize Cu^I and Rh^I Species and Tune Their Reactivity

Jeroen Wassenaar,[†] Maxime A. Siegler,^{‡,§} Anthony L. Spek,[‡] Bas de Bruin,[†] Joost N. H. Reek,^{*,†} and Jarl Ivar van der Vlugt^{*,†}

[†]Supramolecular & Homogeneous Catalysis Group, van 't Hoff Institute for Molecular Sciences, University of Amsterdam, Nieuwe Achtergracht 166, 1018 WV Amsterdam, The Netherlands, and

[‡]Department of Crystal and Structural Chemistry, University of Utrecht, Padualaan 8, 3584 CH Utrecht,

The Netherlands. [§]Current address: Department of Chemistry, John Hopkins University, Baltimore, Maryland

Received February 3, 2010

The high-yielding synthesis and detailed characterization of two well-defined, linkage isomeric tripodal, tetradentate all-phosphorus ligands **1–3** is described. Coordination to Cu^I resulted in formation of complexes **4–6**, for which the molecular structures indicate overall tridentate coordination to the copper atom in the solid state, with one dangling peripheral phosphine. The solution studies suggest fast exchange between the three phosphine side-arms. For these new Cu^I complexes, preliminary catalytic activity in the cyclopropanation of styrene with ethyldiazoacetate (EDA) is disclosed. The anticipated well-defined tetradentate coordination in a C_3 -symmetric fashion was achieved with Rh^I and Ir^I , leading to the overall five-coordinated complexes **7–12**. Complex **11** has the norbornadiene (nbd) ligand coordinated in an unprecedented monodentate 2,3- η^2 mode to Rh. Furthermore, unexpected but very interesting redox-chemistry and reactivity was displayed by the $Rh(Cl)$ -complexes **7** and **8**. Oxidation resulted in the formation of stable Rh^{II} metalloradicals **[7]PF₆** and **[8]PF₆** that were characterized by X-ray crystallography, magnetic susceptibility measurements, cyclic voltammetry, and electron paramagnetic resonance (EPR) spectroscopy. Subsequent redox-reactivity of these metalloradicals toward molecular hydrogen is described, resulting in the formation of Rh^{III} hydride compounds.

Introduction

Constrained metal geometries are often a prerequisite for unusual reactivity and selective metal-mediated catalysis, and this is prevalent as a design principle in both biological and synthetic systems.¹ Multipodal ligand scaffolds are a common approach to enforce formation of metal complexes in well-defined yet unusual and reactive geometries. Notwithstanding the long history of such sterically encumbered, highly regular, multidentate scaffolds, Trofimenko's scorpionates being a classic example², their chemistry as well as the development of new ligand classes continue to receive much attention.³

In particular C_3 -symmetric tripodal skeletons have emerged as attractive frameworks to address specific significant research questions and to steer metal-centered reactivity.^{4–6} Within this family of scaffolds, the pivotal

*To whom correspondence should be addressed. E-mail: j.n.h.reek@uva.nl (J.N.H.R.), j.i.vandervlugt@uva.nl (J.I.v.d.V.).

(1) (a) van der Vlugt, J. I.; Koblenz, T.; Wassenaar, J.; Reek, J. N. H. In *Molecular Encapsulation: Reactions in Constrained Systems*; Miesuet, J.-L.; Brinker, U. H., Eds.; Wiley-VCH: New York, 2010; (b) van der Vlugt, J. I.; Reek, J. N. H. *Angew. Chem., Int. Ed.* **2009**, *48*, 8832–8846. (c) Koblenz, T.; Wassenaar, J.; Reek, J. N. H. *Chem. Soc. Rev.* **2008**, *37*, 247–262. (d) Kuil, M.; Soltner, T.; van Leeuwen, P. W. N. M.; Reek, J. N. H. *J. Am. Chem. Soc.* **2006**, *128*, 11344–11345. (e) Drauz, K.; Waldmann, H. *Enzyme Catalysis in Organic Synthesis: A Comprehensive Handbook*, 2nd ed.; Wiley-VCH: New York, 2002.

(2) Trofimenko, S. *Chem. Rev.* **1993**, *93*, 943–980.

(3) (a) Moberg, C. *Angew. Chem., Int. Ed.* **1998**, *37*, 248–268. (b) Kuzu, I.; Krummenacher, I.; Meyer, J.; Armbruster, F.; Breher, F. *Dalton Trans.* **2008**, 5836–5865.

(4) Monoanionic tris(phosphino)borates: (a) Lu, C. C.; Saouma, C. T.; Day, M. W.; Peters, J. C. *J. Am. Chem. Soc.* **2007**, *129*, 4–5. (b) Betley, T. A.; Peters, J. C. *Inorg. Chem.* **2003**, *42*, 5074–5084. (c) Shapiro, I. R.; Jenkins, D. M.; Thomas, J. C.; Day, M. W.; Peters, J. C. *Chem. Commun.* **2001**, 2152–2153. (d) Turculet, L.; Feldman, J. D.; Tilley, T. D. *Organometallics* **2004**, *23*, 2488–2502. Related tris(phosphino)silanes: Mankad, N. P.; Whited, M. T.; Peters, J. C. *Angew. Chem., Int. Ed.* **2007**, *46*, 5768–5771. Whited, M. T.; Mankad, N. P.; Lee, Y.; Oblad, P. F.; Peters, J. C. *Inorg. Chem.* **2009**, *48*, 2507–2517. Lee, Y.; Mankad, N. P.; Peters, J. C. *Nat. Chem.* **2010**, *2*, DOI: 10.1038/nchem.660.

(5) Neutral tris(phosphino)boranes: (a) Sircoglou, M.; Bontemps, S.; Bouhadir, G.; Saffon, N.; Miqueu, K.; Gu, W. X.; Mercy, M.; Chen, C. H.; Foxman, B. M.; Maron, L.; Ozerov, O. V.; Bourissou, D. *J. Am. Chem. Soc.* **2008**, *130*, 16729–16738. (b) Bontemps, S.; Bouhadir, G.; Gu, W.; Mercy, M.; Chen, C. H.; Foxman, B. M.; Maron, L.; Ozerov, O. V.; Bourissou, D. *Angew. Chem., Int. Ed.* **2008**, *47*, 1481–148. (c) Bontemps, S.; Bouhadir, G.; Dyer, P. W.; Miqueu, K.; Bourissou, D. *Inorg. Chem.* **2007**, *46*, 5149–5151. For other C_3 -symmetric neutral phosphorus-based ligands, see: (d) Grutters, M. M. P.; van der Vlugt, J. I.; Pei, Y.; Mills, A. M.; Lutz, M.; Spek, A. L.; Müller, C.; Moberg, C.; Vogt, D. *Adv. Synth. Catal.* **2009**, *351*, 2199–2208. (e) Ionescu, G.; van der Vlugt, J. I.; Abbenhuis, H. C. L.; Vogt, D. *Tetrahedron: Asymmetry* **2006**, *16*, 3970–3975. (f) van der Vlugt, J. I.; Ackersstaff, J.; Dijkstra, T. W.; Mills, A. M.; Kooijman, H.; Spek, A. L.; Meetsma, A.; Abbenhuis, H. C. L.; Vogt, D. *Adv. Synth. Catal.* **2004**, *346*, 399–412.

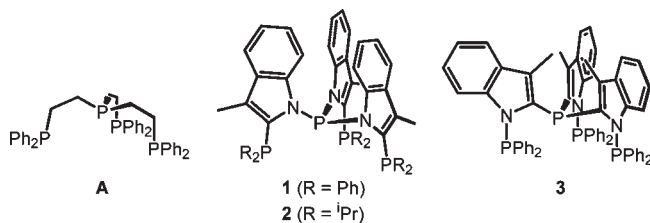


Figure 1. Tetraphosphine **A** and the new indole-based all-phosphorus tripodal ligands **1–3**.

atom can either be a spectator entity (tridentate ligation) or a donor atom binding to the metal fragment (tetradentate ligation). C_3 -symmetric tripodal, tetradentate ligands that feature an all-phosphorus coordination sphere are rare.^{7,8} Bianchini et al. studied the coordination chemistry of ligand **A** toward Rh,^{9,10} while Field and co-workers recently described Fe(0) and Ru(0) dinitrogen complexes with the *iso*-propyl-derivative of ligand **A** (see Figure 1).¹¹

The applicability of such C_3 platforms for the formation of (late) transition metal complexes is related to the confined geometry dictated onto the metal center. Subtle electronic influences, for example, of the pivotal atom and the side arm donor groups, and the steric impact of peripheral fragments govern the resulting reactivity of (in particular) low-valent metal species.

Convergent synthetic methodologies to prepare symmetric tripodal scaffolds are available but most of the reported examples lack opportunities to easily access a number of electronic and structural variations through modular synthesis. Moreover, despite the highly symmetric nature of the C_3 -symmetric backbone, *rigidity* is scarcely employed as an important design feature for tripodal ligand systems.¹² However, flexidentate behavior¹³ of the scaffold is undesirable when targeting restricted geometric structures to study the effects on corresponding metal centers and their reactivity.

We recently reported on the use of 3-methylindole as rigid scaffold for the construction of hybrid bidentate ligand IndolPhos (Figure 2), a chiral phosphine-phosphoramidite

species, which was successfully applied in homogeneous catalysis. Excellent results were obtained in the synthesis of Roche ester derivatives by asymmetric hydrogenation.¹⁴ We have extended this work to chiral phosphole-phosphoramidite ligands, for use in Pd-catalyzed asymmetric allylic alkylation.¹⁵

We next wondered if we could expand on this motif to arrive at sterically demanding tripodal tetraphosphine ligands (PP₃) and to see if the corresponding metal complexes with such enforcing frameworks display unusual characteristics. Such scaffolds should enforce conformational rigidity and in particular unusual geometries around (late) transition metal centers, potentially leading to new reactivity. Here we report the synthesis of new C_3 -symmetric tripodal tetraphosphine ligands **1–3**, capitalizing on previously developed modular synthetic strategies for IndolPhos, and their complexes with Cu^I, Rh^I, and Ir^I. Reactivity studies of these complexes show facile oxidation of the Rh^I complexes, resulting in stable Rh^{III} metalloradicals. The dominant ligand structure results in highly distorted square-pyramidal geometries. This in turn is the onset for unusual subsequent reactivity of these paramagnetic species with dihydrogen to yield Rh^{III} hydride compounds.

Results and Discussion

We set out to construct PP₃ ligand **1**, which features a central phosphorus atom connected to three indole N-fragments.¹⁶ This ligand is straightforwardly synthesized from the reported 2-diphenylphosphino-3-methylindole via a base-promoted reaction with PCl₃. In the corresponding ³¹P NMR spectrum, the signal for the pivotal P-atom was observed as a quartet at δ 73.7 ppm, while a doublet was observed at δ –29.6 ppm for the peripheral PPh₂ units, with a large coupling constant J_{P-P} of 197 Hz. To demonstrate the versatile nature of these scaffolds, we also prepared and fully characterized the tris-PⁱPr₂ analogue **2** of compound **1**. It shows two distinct peaks in the ³¹P NMR spectrum at δ –9.9 (PP₃) and 67.3 ppm (PP₃) with the expected relative integration ratio of 1:3. Because of the rigid, sterically encumbered conformation of ligand **2**, the two isopropyl groups on each peripheral phosphine fragment are inequivalent, even in solution, as indicated by the observation of two ¹Pr –CH group resonances in the ¹H NMR spectrum. We ascribe this observation to a locked inequivalent conformation of the ¹Pr groups, caused by strong steric interactions between the neighboring P(ⁱPr)₂ moieties. Four different ¹Pr-based methyl signals in a 1:1:1:1 ratio are expected, based on this inequivalency of the two ¹Pr groups per P(ⁱPr)₂ moiety, combined with the diastereotopicity of the two Me groups within each ¹Pr moiety and the overall C_3 symmetry of the ligand (leading to three equivalent P(ⁱPr)₂ moieties). Two of these signals apparently overlap, since we observe three ¹Pr methyl signals

(6) Monoanionic tris(indolylphosphino)methane: (a) Ciclosi, M.; Estevan, F.; Lahuerta, P.; Passarelli, V.; Pérez-Prieto, J.; Sanau, M. *Dalton Trans.* **2009**, 2290–2297. (b) Ciclosi, M.; Estevan, F.; Lahuerta, P.; Passarelli, V.; Pérez-Prieto, J.; Sanau, M. *Adv. Synth. Catal.* **2008**, *350*, 234–236. (c) Ciclosi, M.; Lloret, J.; Estevan, F.; Lahuerta, P.; Sanau, M.; Pérez-Prieto, J. *Angew. Chem., Int. Ed.* **2006**, *45*, 6741–6744. For a report on the same scaffold but lacking the relevant pivotal C-H activation: Ciclosi, M.; Lloret, J.; Estevan, F.; Sanaú, M.; Pérez-Prieto, J. *Dalton Trans.* **2009**, 5077.

(7) Baker, M. J.; Pringle, P. G. *J. Chem. Soc., Chem. Commun.* **1993**, 314–316.

(8) King, R. B.; Kapoor, R. N. *J. Am. Chem. Soc.* **1969**, *91*, 5191–5192.

(9) (a) Bianchini, C.; Masi, D.; Meli, A.; Peruzzini, M.; Zanobini, F. *J. Am. Chem. Soc.* **1988**, *110*, 6411–6423. (b) Bianchini, C.; Meli, A.; Peruzzini, M.; Zanobini, F. *Organometallics* **1990**, *9*, 1155–1160. (c) Bianchini, C.; Mealli, C.; Peruzzini, M.; Zanobini, F. *J. Am. Chem. Soc.* **1987**, *109*, 5548–5549. (d) Bianchini, C.; Meli, A.; Peruzzini, M.; Vacca, A.; Zanobini, F. *Organometallics* **1987**, *6*, 2453–2455.

(10) Venanzi reported chemistry with an aryl-bridged analogue of PP₃ ligand **A**: Dawson, J. W.; Venanzi, L. M. *J. Am. Chem. Soc.* **1968**, *90*, 7229–7233.

(11) Field, L. D.; Guest, R. W.; Vuong, K. Q.; Dalgarno, S. J.; Jensen, P. *Inorg. Chem.* **2009**, *48*, 2246–2253.

(12) (a) Foltz, C.; Enders, M.; Bellemin-Lapponnaz, S.; Wadepohl, H.; Gade, L. H. *Chem.—Eur. J.* **2007**, *13*, 5994–6008. (b) Ward, B. D.; Bellemin-Lapponnaz, S.; Gade, L. H. *Angew. Chem., Int. Ed.* **2005**, *44*, 1668–1671. (c) Bellemin-Lapponnaz, S.; Gade, L. H. *Angew. Chem., Int. Ed.* **2002**, *41*, 3473–3475.

(13) We prefer the term flexidentate over hemilabile, as the former more strongly implies bidirectional coordination character.

(14) (a) Wassenaar, J.; Reek, J. N. H. *Dalton Trans.* **2007**, 3750–3753. (b) Wassenaar, J.; Kuil, M.; Reek, J. N. H. *Adv. Synth. Catal.* **2008**, *350*, 1610–1614. (c) Wassenaar, J.; Reek, J. N. H. *J. Org. Chem.* **2009**, *74*, 8403–8406.

(15) (a) Wassenaar, J.; van Zutphen, S.; Mora, G.; Le Floch, P.; Siegler, M.; Spek, A. L.; Reek, J. N. H. *Organometallics* **2009**, *28*, 2724–2734. (b) Wassenaar, J.; Jansen, E.; van Zeist, W.-J.; Bickelhaupt, F. M.; Siegler, M. A.; Spek, A. L.; Reek, J. N. H. *Nat. Chem.* **2010**, *2*, 417–421.

(16) Wassenaar, J.; de Bruin, B.; Siegler, M. A.; Spek, A. L.; Reek, J. N. H.; van der Vlugt, J. I. Facile oxidation of Rh(I) and Ir(I) complexes derived from new tripodal tetradentate ligands (INOR-260). *Abstracts of Papers*, 238th ACS National Meeting, Washington, DC, United States, August 16–20, 2009.

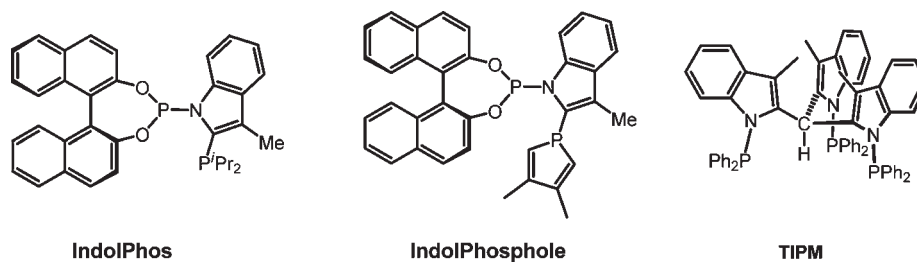
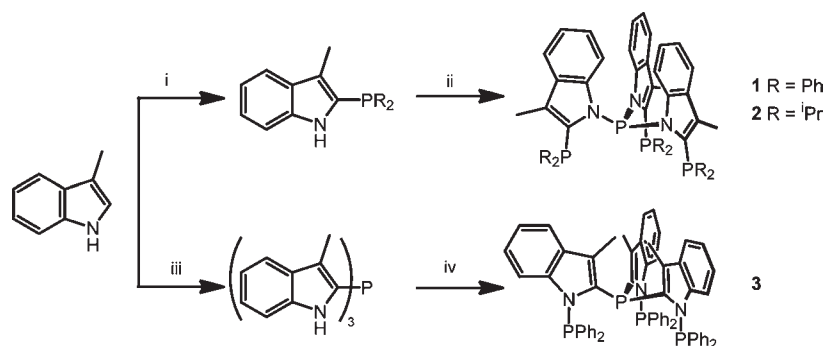


Figure 2. Recently developed hybrid ligand class IndolPhos,¹⁴ the corresponding phospholane-phosphoramidite used in asymmetric allylic alkylation,¹⁵ and Lahuerta's tris(indolylphosphine)methane ligand.⁶

Scheme 1. Synthesis of Tripodal Ligands 1–3^a



^a Conditions: (i) *n*-BuLi, THF, $-78\text{ }^{\circ}\text{C}$; CO_2 ; *t*-BuLi; CIPR_2 ($\text{R} = \text{Ph}$, ^iPr). (ii) *n*-BuLi, THF, $-78\text{ }^{\circ}\text{C}$; PCl_3 . (iii) *n*-BuLi, THF, $-78\text{ }^{\circ}\text{C}$; CO_2 ; *t*-BuLi; PCl_3 . (iv) *n*-BuLi, THF, $-78\text{ }^{\circ}\text{C}$; CIPPh_2 .

in a 2:1:1 ratio. One ^iPr methyl group is shifted to high field ($\delta -0.06$ ppm), likely a result of anisotropic shielding from the aromatic indole rings. An independent synthesis to obtain ligand **1** was recently reported by the group of Pérez-Prieto,¹⁷ albeit that the original, unoptimized procedure for the preparation of 2-diphenylphosphino-3-methylindole was employed whereas the applied in situ CO_2 protection methodology reported for IndolPhos is superior.¹⁶

Conversely, ligand **3** bears a bridgehead phosphorus atom that is connected at the 2-position of 3-methylindole, thus reversing the overall pattern and synthetic methodology (Scheme 1).¹⁸ Capping of PCl_3 with 3 equiv of 2-lithioindole,¹⁹ employing in situ protection of the nitrogen using CO_2 ,²⁰ followed by phosphorylation of the nitrogen gave the desired product **3**, the linkage isomer of **1**, in good yield, with chemical shifts at $\delta -75.1$ (quartet) and 37.3 ppm (doublet), with a coupling constant $J_{\text{P-P}}$ of 159 Hz.

The two linkage isomers show remarkable differences in the NMR spectra; the $\Delta\delta$ for the pivotal-phosphorus atom is ~ 150 ppm, while the peripheral phosphines (PPh_2 only) span a range of 66 ppm between ligand **1** and **3**. This suggests strikingly different geometric and/or electronic environments for the two types of P-atoms in each ligand. Single crystals for

species **1** and the tris-oxide of **3** were grown from $\text{CDCl}_3\text{-Et}_2\text{O}$ and THF-hexane, respectively (see Supporting Information). For compound **1**,¹⁶ the obtained intramolecular distances and angles are very similar to the structure reported by Pérez-Prieto.¹⁷ Oxidation of the peripheral phosphines occurred in solution during the slow crystallization of **3**. Although this compound is stable when stored as a solid, this observation might indicate a subtle difference in the electronic properties of the phosphines in **1** and **3**. The C_3 -symmetric nature of these ligand scaffolds is immediately apparent, as well as the helical feature enforced by the sterically encumbered side groups. The lone pair on the central P_1 atom points inward with respect to the cavity created by the three bulky arms. The overall C_3 -symmetry and related basket-shaped configuration likely also dominates in solution as a result of the rigid ligand architecture. This is indicated by the large coupling constant $J_{\text{P-P}}$ between the inequivalent P-atoms, with values of 197 and 159 Hz for **1** and **3**, respectively.

Coordination Chemistry to Cu^I. We initially focused on Cu as the metal of choice for these PP_3 ligands, to investigate its coordination chemistry as well as potential catalytic applications (Scheme 2).

Reaction of ligands **1–3** with $[\text{Cu}(\text{cod})(\mu\text{-Cl})_2]$ led to the light-yellow solids $[\text{CuCl}(\mathbf{1})]$ (**4**), $[\text{CuCl}(\mathbf{2})]$ (**5**), and $[\text{CuCl}(\mathbf{3})]$ (**6**) in moderate to excellent yields, which showed some broadened signals in the NMR spectra. The ^{31}P NMR spectrum of **4** showed a quartet at $\delta 58.70$ and a doublet at -27.68 ppm, with a $J_{\text{P-P}}$ coupling constant of 198 Hz, suggesting on average C_3 -symmetry in solution on the NMR time scale at rt. Cooling of the sample led to broadening of all signals, but unfortunately the dynamic coordination process could not be frozen out. At $-60\text{ }^{\circ}\text{C}$, complete coalescence of the signals was still not observed in CD_2Cl_2 . Similar spectral features at rt

(17) During the final writing stage of our current paper, a Note appeared with the independent synthesis of compound **1** as well as some coordination chemistry with Pd and characterization of the Rh(Cl)-complex (similar to our species **7**); Penno, D.; Koshevoy, I. O.; Estevan, F.; Sanaú, M.; Angeles Ubeda, M.; Pérez-Prieto, J. *Organometallics* **2010**, *29*, 703–706.

(18) A preliminary account of this work has been communicated recently: Wassenaar, J.; de Bruin, B.; Siegler, M. A.; Spek, A. L.; Reek, J. N. H.; van der Vlugt, J. I. *Chem. Commun.* **2010**, *46*, 1432–1434.

(19) Tris-2-(3-methylindolyl)phosphine has been reported, see: Yu, J. O.; Browning, C. S.; Farrar, D. H. *Chem. Commun.* **2008**, 1020–1022.

(20) Katritzky, A. R.; Akutagawa, K.; Jones, R. A. *Synth. Commun.* **1988**, *18*, 1151–1158.

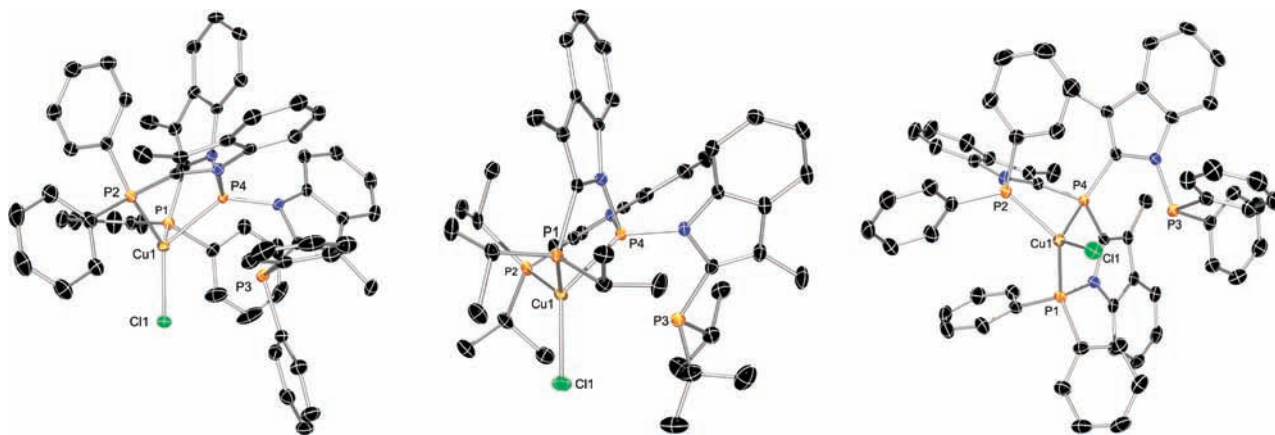
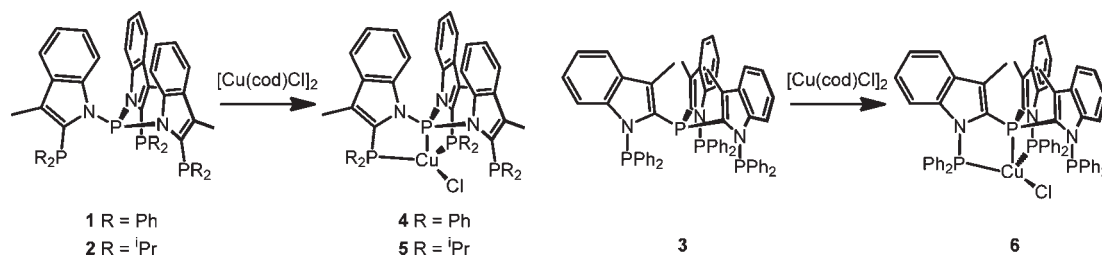


Figure 3. ORTEP plots (50% probability displacement ellipsoids) of Cu^I-complexes **4** (left), **5** (middle), and **6** (right). Hydrogen atoms and solvent molecules are omitted for clarity. Selected bond lengths (Å) and angles (deg), for **4**: Cu₁–P₁ 2.2628(5), Cu₁–P₂ 2.2468(6), Cu₁···P₃ 3.7163(6), Cu₁–P₄ 2.3292(5), Cu₁–Cl₁ 2.2277(5); P₁–Cu₁–Cl₁ 116.93(2), P₂–Cu₁–Cl₁ 120.17(2), P₄–Cu₁–Cl₁ 123.82(2), P₁–Cu₁–P₂ 118.02(2), P₁–Cu₁–P₄ 83.81(2), P₂–Cu₁–P₄ 83.91(2). For **5**: Cu₁–P₁ 2.2645(5), Cu₁–P₂ 2.2632(5), Cu₁···P₃ 3.8296(6), Cu₁–P₄ 2.2994(5), Cu₁–Cl₁ 2.2645(5); P₁–Cu₁–Cl₁ 105.78(2), P₂–Cu₁–Cl₁ 115.36(2), P₄–Cu₁–Cl₁ 133.52(2), P₁–Cu₁–P₂ 129.12(2), P₁–Cu₁–P₄ 86.65(2), P₂–Cu₁–P₄ 85.99(2). For **6**: Cu₁–P₁ 2.2598(5), Cu₁–P₂ 2.2689(5), Cu₁···P₃ 3.9083(5), Cu₁–P₄ 2.2841(7), Cu₁–Cl₁ 2.2436(7); P₁–Cu₁–Cl₁ 115.82(3), P₂–Cu₁–Cl₁ 116.43(2), P₄–Cu₁–Cl₁ 125.02(2), P₁–Cu₁–P₂ 120.79(2), P₁–Cu₁–P₄ 85.90(2), P₂–Cu₁–P₄ 86.16(2).

Scheme 2. Complexation of Novel Tripodal Ligands **1–3** to Cu^I



and $-60\text{ }^{\circ}\text{C}$ were observed for complex **5** and **6**. Single crystals suitable for X-ray crystallographic analysis were obtained from CH_2Cl_2 -toluene/hexane for complex **4–6** (see the molecular structures in Figure 3).

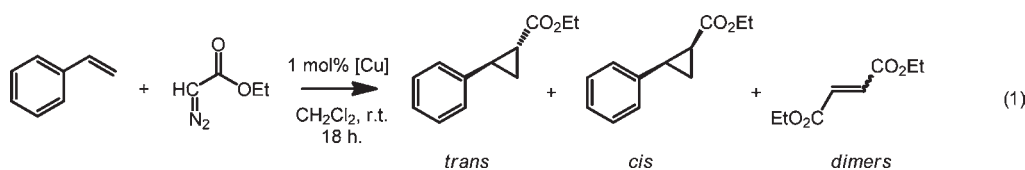
The Cu^I ions in all complexes adopt distorted tetrahedral geometries, with coordination to *two* peripheral PR₂ groups, the central phosphorus atom of the tripodal ligand and to the chloride coligand. The total sums of all angles are 647° (**4**), 656° (**5**), and 650° (**6**), respectively. Tetradentate coordination of the ligands is unfavorable as this would lead to 20 electron complexes. Hence, there is no element of symmetry left in the molecules, as one phosphine unit is dangling in the solid state, while there is rapid exchange of the peripheral donor units in solution according to the NMR studies. The Cu–P distances in complex **4** vary from 2.2468(5) Å for Cu–P_{periphery} to 2.3292(5) Å for Cu–P_{central}, in the range of typical Cu^I-phosphine complexes.²¹ The remaining Cu···P₃ distance is 3.7163(6) Å and Cu–Cl is 2.2277(5) Å. The two P_{central}–Cu–P_{periphery} angles are 83.81(2) and 83.91(2) $^{\circ}$, while the P_{central}–Cu–Cl angle is much larger at 123.82(2) $^{\circ}$. This again is a clear indication of the constrained geometry of the formally tripodal ligand scaffold.

Complex **5** exhibits an even more distorted geometry indicated by a large P_{central}–Cu–Cl angle of 133.52(2) $^{\circ}$. The slightly more flexible nature of the ligand of complex **6** allows for a more open geometry, which is indicated by a larger Cu···P₃ distance of 3.9083 Å. This may be the reason for the lower selectivity in the Cu^I catalyzed cyclopropanation as the Cu ion is less shielded by the ligand framework (vide infra).

Cu^I Catalyzed Cyclopropanation. A first indication of the catalytic applicability of the Cu-complexes **4–6** was obtained by examining the Cu-catalyzed cyclopropanation of styrene with ethyldiazoacetate (EDA) after in situ removal of the chloride using AgOTf (Table 1).²² All complexes gave active catalysts for this reaction and quantitative conversion (based on EDA) after 18 h reaction time, with the Cu-catalyst containing the more rigid ligand **1** giving the highest *trans* to *cis* ratio of 70/30 (complex **4**). However, significant amounts (up to 43%) of diethyl maleate and fumarate are formed as a result of Cu-catalyzed dimerization of EDA. Interestingly, complex **6**, containing the linkage isomeric ligand **3**, gives lower amounts of dimers (28%, entry 3). This shows that the subtle differences in ligand structure between these linkage isomers lead to altered reactivity of the resulting metal complexes. Control experiments with [CuOTf]₂·benzene give a 60/40 *trans/cis* ratio and only 12% dimer formation (entry 4). Apparently the ligands

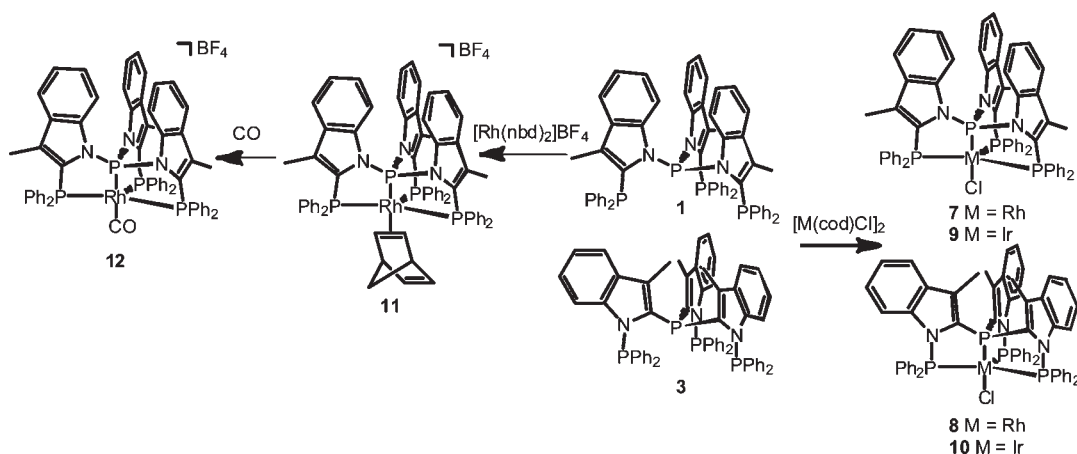
(21) For recent examples, see: (a) van der Vlugt, J. I.; Pidko, E. A.; Vogt, D.; Lutz, M.; Spek, A. L.; Meetsma, A. *Inorg. Chem.* **2008**, *47*, 4442–4444. (b) van der Vlugt, J. I.; Pidko, E. A.; Vogt, D.; Lutz, M.; Spek, A. L. *Inorg. Chem.* **2009**, *48*, 7513–7515. (c) Sircoglou, M.; Bontemps, S.; Mercy, M.; Miqueu, K.; Ladeira, S.; Saffon, N.; Maron, L.; Bouhadir, G.; Bourissou, D. *Inorg. Chem.* **2010**, *49*, 3983–3990.

(22) (a) Davies, H. M. L.; Hedley, S. J. *Chem. Soc. Rev.* **2007**, *36*, 1109–1119. (b) Kirmse, W. *Angew. Chem., Int. Ed.* **2003**, *42*, 1088–1093.

Table 1. Catalytic Cyclopropanation of Styrene and EDA (Ethyl Diazoacetate) Using New Cu^I-Complexes 4–6^a

entry	catalyst	conversion ^b	yield ^{b, c}	% <i>trans/cis</i> ratio ^b	% dimers ^b
1	[Cu(1)]OTf (4 ^{Ph})	100	57	70/30	43
2	[Cu(2)]OTf (5 ^{iPr})	100	66	69/31	34
3	[Cu(3)]OTf (6)	100	72	66/34	28
4	[CuOTf] ₂ -benzene	100	88	60/40	12

^a Ratio styrene:EDA:catalyst = 800:100:1; temperature = 25 °C; reaction time = 18 h; solvent: CH₂Cl₂. ^b Determined by ¹H NMR spectroscopy. ^c Combined yield of *cis* and *trans*-isomers

Scheme 3. Coordination of Ligands 1 and 3 toward Rh and Ir Precursors, Leading to Complexes 7–12

enforce a slight increase in selectivity toward the *trans* product, but further ligand design will be necessary to enable a semi-enclosed coordination of the Cu-center with potentially altered reactivity and selectivity.

Coordination Chemistry to Rh and Ir. Strikingly, C₃-symmetric scaffolds have hardly been used with Rh to date,^{4d,6a,17,23} yet the combination of a rigid ligand structure and an active protected metal site might yield interesting reactivity. The use of rigid ligand scaffolds is attractive and necessary to enforce a specific metal geometry, both to restrict and direct the desired reactivity of the metal center. In conjunction with tetradentate coordination, conformational freedom is minimized, thus paving the way for rational design and targeted reactivity. If encapsulation of the metal center by the C₃-symmetric ligand appears effective with the archetypical M^I oxidation state (M = Rh and Ir), such ligand frameworks might also open up opportunities to synthesize and stabilize the open-shell derivatives (M^{II}) and to study their characteristics.

Therefore, to further investigate the potential of the new linkage isomeric ligands 1 and 3, each ligand was reacted with suitable Rh and Ir precursors (Scheme 3). Complexation with either neutral Rh or Ir was achieved by reaction of stoichiometric amounts of the respective ligand with [Rh(cod)₂(μ-Cl)]₂ or [Ir(cod)₂(μ-Cl)]₂. The resulting complexes 7 [RhCl(1)],¹⁷ 8 [RhCl(3)], 9 [IrCl(1)], and 10 [IrCl(3)] were fully characterized by NMR spectroscopy, elemental analysis, and high resolution mass spectrometry. It should be noted that formation of compound 10 was sluggish, compared to the other three species. The ³¹P NMR spectrum for 7 consists of a doublet-of-quartets at δ 131.8 ppm (Δδ is 58.1 ppm) for the central P-atom (*J*_{Rh-P} coupling constant of 170 Hz), and the combined peripheral phosphorus-units are present at δ 5.7 ppm as a doublet-of-doublets, with a *J*_{P-P} coupling constant of 30 Hz (*J*_{Rh-P}: 138 Hz). Surprisingly, attempts to coordinate the ^tPr analogue (ligand 2) to, for example, the Rh-precursor failed, presumably because of excessive steric crowding around the metal center.

Single crystals for both Rh-complexes 7 and 8 were obtained by slow diffusion of hexane into a tetrahydrofuran (THF) or dichloromethane (DCM) solution (see Supporting Information for details). Both structures display a distorted trigonal bipyramidal geometry. The respective Rh–P distances including the axially coordinated pivotal P₁-donor of 2.1124(4) Å (7) and 2.1592(7) Å

(23) Rh-complexes with the aliphatic tripodal tetradentate ligand P(CH₂CH₂PPh₂)₃ have been reported, see ref 9 and: (a) Di Vaira, M.; Ehes, M. P.; Peruzzini, M.; Stoppioni, P. *Eur. J. Inorg. Chem.* **2000**, 2193–2198. (b) Heinekey, D. M.; van Roon, M. *J. Am. Chem. Soc.* **1996**, *118*, 12134–12140. (c) Bianchini, C.; Elsevier, C. J.; Ernsting, J. M.; Peruzzini, M.; Zanobini, F. *Inorg. Chem.* **1995**, *34*, 84–92. (d) Taqui Khan, M. M.; Martell, A. E. *Inorg. Chem.* **1974**, *13*, 2961–2966.

(8) are slightly shorter than those found for the equatorially coordinated side arm phosphines (at ~ 2.29 – 2.36 Å). As with the structure for ligand **1**, independent synthesis and solid-state structure determination of **7** was reported by Pérez-Prieto and co-workers.¹⁷ Their data are very similar to ours, with subtle but noticeable differences most likely reflecting slight differences in crystal packing combined with different collection temperatures (room temperature vs 110 K in our case).

Contrary to pyrrolyl-based phosphorus ligands, which tend to act as ‘pseudophosphites’ and as a result show longer Rh–P bond lengths compared to traditional phosphine ligands,²⁴ the respective bridgehead P-atom in complexes **7** and **8** appear not to participate in π -backdonation, thus resembling more classical $\text{P}(\text{NR}_2)_3$ donors.²⁵ The latter is further evidenced by the absence of elongation of the P_1 –N bonds in the complexes compared to the free ligand. It should be noted that the deviation from ideal tbp geometry structure is somewhat larger for **7** (τ -value: 0.80) than for complex **8** (τ -value: 0.93).²⁶ This can be explained by the even more rigid ligand framework of **1**.

Unprecedented Monodentate 2,3- η^2 -nbd Coordination to Rh. A cationic analogue of the RhCl-complex **7** with ligand **1** was also attainable, by using $[\text{Rh}(\text{nbd})_2]\text{BF}_4$ (nbd = norbornadiene) as precursor. This led to the formation of an orange-red colored species $[\text{Rh}(\text{1})(\text{nbd})]\text{BF}_4$ (**11**), which also exhibited a clear ^{31}P NMR spectrum (δ 132.4 and 6.4 ppm) and a highly ordered ^1H NMR spectrum, with unambiguous signals for a single coordinated nbd coligand with a rare 2,3- η^2 -monodentate coordination mode. This is evidenced by the observation of two sets of signals for the diene protons in the ^1H NMR spectrum at 5.37 and 4.55 ppm for the η^2 coordinated double bond, and at 6.33 and 6.25 ppm for the non-coordinated double bond. To our knowledge this is the first Rh(nbd)-complex wherein the norbornadiene acts as a monodentate ligand, leaving one double bond uncoordinated, which must be a result of the coordinating power of the multidentate phosphorus ligand. In addition, all diene signals are doubled, because of the chiral C_3 -symmetric environment imposed by the tetraphosphine ligand. To further understand the bonding nature in this species, we performed density functional theory (DFT) calculations (see Figure 4). The optimized structure shows just *one* coordinated double bond of the nbd ligand, which is coordinated in the anticipated *endo*-conformation. This is in agreement with NMR spectroscopic observations wherein only two diene protons are shifted upfield. The intramolecular distance Rh–($\text{C}_1=\text{C}_2$) for the coordinated double bond is approximately 2.3 Å, whereas the distance of the free double bond ($\text{C}_3=\text{C}_4$) to the Rh-center is beyond bonding range at ~ 3.6 Å in the DFT optimized structure.

Substitution to Give Monocarbonyl Complex 12. Complex **11** proved to be unreactive toward molecular hydrogen, as no hydrogenation of the diene was observed. This can be understood by the lack of vacant sites on the metal

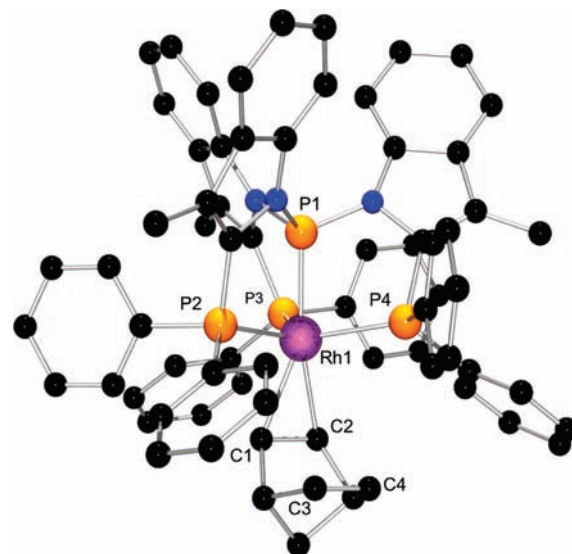


Figure 4. DFT optimized geometry for complex **11**, $[\text{Rh}(\text{1})(\text{nbd})]\text{BF}_4$, with an 2,3- η^2 -monodentate coordination of the norbornadiene fragment.

for hydrogen coordination. This is due to effective shielding of the metal by the rigid ligand framework. Notwithstanding this observation, substitution chemistry proceeded smoothly as the formation of, for example, the corresponding CO-complex, $[\text{Rh}(\text{1})(\text{CO})]\text{BF}_4$ (**12**), was facile upon exposure of complex **11** under 25 bar CO at rt in CH_2Cl_2 , yielding the corresponding orange-colored monocarbonyl complex. The ^{31}P NMR spectrum indicated a downfield shift of the peripheral phosphines to 16.3 ppm ($\Delta\delta = 10$ ppm) compared to nbd-complex **11**, most probably resulting from the stronger π -acidic character of the CO ligand. The FT-IR spectrum showed one strong band at ν_{CO} 2000 cm^{-1} . This is in the expected range for five-coordinated cationic Rh(CO)-species²⁷ and is somewhat higher than in the related $[\text{Rh}(\text{A})(\text{CO})]\text{BF}_4$ complex (ν_{CO} 1985 cm^{-1}), because of the electron-accepting nature of the indole based ligand **1** compared to the alkyl based ligand **A**.⁹ However, judging from the ν_{CO} value, the indolylphosphine fragment is definitely not a strong π -acceptor, unlike the pyrrolylphosphine analogues. Single crystals of **12** suitable for X-ray crystallography were obtained from slow diffusion of hexane into a CH_2Cl_2 solution (Figure 5). The structure exhibits a distorted trigonal bipyramidal geometry (τ -value: 0.75), similar to the corresponding chloride complex **7**. The Rh_1 – P_4 distance is 2.1978(6) Å, which is 0.085 Å longer than in the more electron rich chloride complex **7**. This indicates that even though the ligand may be a weaker π -acid compared to pyrrolyl-analogues, the pivotal phosphorus donor P_4 does participate in π -backbonding.

Reactivity of Rh^I Complexes toward Acids and Alkylating Agents. In marked contrast with the aforementioned work on the Rh^I complex of ligand **A**,⁹ we were unsuccessful in obtaining a stable Rh^{III} dihydrido-species or subsequent monohydrido complexes with ligands **1** or **3**, by treatment of the cationic $[\text{Rh}^{\text{III}}(\text{H})(\text{Cl})]\text{OTf}$ species **13**, obtained by reaction of **7** with triflic acid, with excess

(24) Moloy, K. G.; Petersen, J. L. *J. Am. Chem. Soc.* **1995**, *117*, 7696–7710.

(25) Crabtree, R. H. In *The Organometallic Chemistry of the Transition Metals*, 3rd ed.; John Wiley & Sons Inc.: New York, 2001; pp 91–95.

(26) Addison, A. W.; Rao, T. N.; Reedijk, J.; van Rijn, J.; Verschoor, G. C. *J. Chem. Soc., Dalton. Trans.* **1984**, 1349–1356.

(27) (a) de Bruin, B.; Donners, J. J. J. M.; de Gelder, R.; Smits, J. M. M.; Gal, A. W. *Eur. J. Inorg. Chem.* **1998**, 401–406. (b) Gambaro, J. J.; Hohman, W. H.; Meek, D. W. *Inorg. Chem.* **1989**, *28*, 4154–4159.

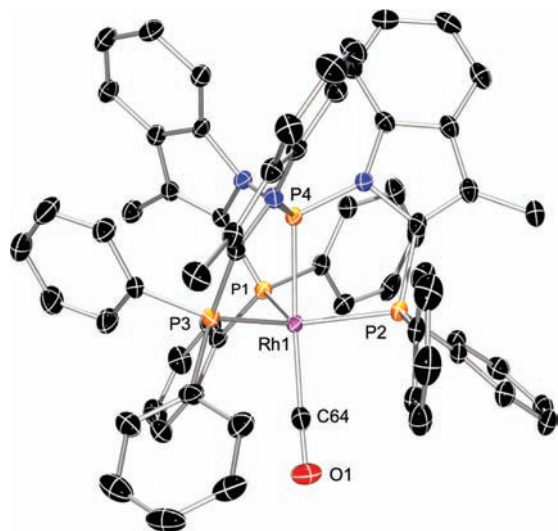
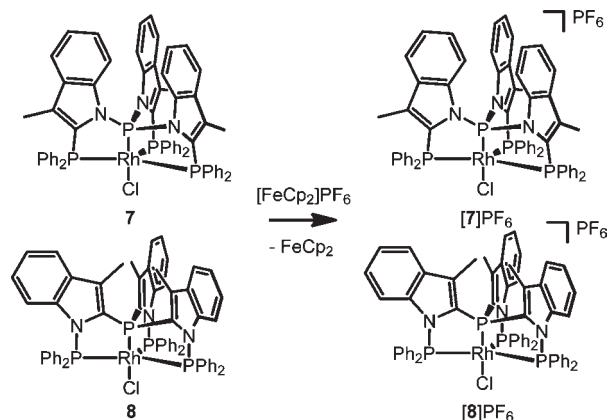


Figure 5. ORTEP plot (50% probability displacement ellipsoids) of the cationic portion of complex **12**. Hydrogen atoms, the BF_4^- anion, and solvent molecules are omitted for clarity. Selected bond lengths (\AA) and angles (deg): $\text{Rh}_1\text{-P}_1$ 2.3545(6), $\text{Rh}_1\text{-P}_2$ 2.3174(7), $\text{Rh}_1\text{-P}_3$ 2.1978(6), $\text{Rh}_1\text{-P}_4$ 2.1978(6), $\text{Rh}_1\text{-C}_{64}$ 1.925(3), $\text{C}_{64}\text{-O}_1$ 1.119(3); $\text{P}_1\text{-Rh}_1\text{-C}_{64}$ 108.84(7), $\text{P}_2\text{-Rh}_1\text{-C}_{64}$ 92.35(7), $\text{P}_3\text{-Rh}_1\text{-C}_{64}$ 95.64(7), $\text{P}_4\text{-Rh}_1\text{-C}_{64}$ 168.64(7), $\text{P}_1\text{-Rh}_1\text{-P}_4$ 82.52(2), $\text{P}_2\text{-Rh}_1\text{-P}_4$ 81.75(2), $\text{P}_3\text{-Rh}_1\text{-P}_4$ 79.81(2), $\text{Rh}_1\text{-C}_{64}\text{-O}_1$ 172.6(2).

NaBH_4 (see Supporting Information). Furthermore, RhCl -complexes **7** and **8** have failed to show any appreciable reactivity toward methyl- or phenyllithium, because of an unusual stability of the $\text{Rh}\text{-Cl}$ bond, hence precluding the synthesis of species featuring a $\text{Rh}\text{-C}$ bond. This is in contrast with the results reported with ligand **A**, where Cl could be displaced for alkyl fragments via salt metathesis. This could be an indication that the *trans* influence of the phosphorus bridgehead in **1** and **3** is small compared to the central alkylphosphine fragment in **A**.

Oxidation to Rh^{II} . Rh -chemistry is dominated by the coordination chemistry of Rh^{I} and Rh^{III} , while the intermediate oxidation state of Rh^{II} is largely considered exotic.²⁸ However, a growing body of evidence is suggesting that such odd-electron species might play an important role in the transformation of organic compounds.²⁹ In fact, dinuclear *bis*- Rh^{II} species catalyze the (Doyle-type) cyclopropanation of alkenes with diazo compounds.³⁰ Mononuclear paramagnetic Rh^{II} and Ir^{II} species are studied to a lesser extent, but these compounds also reveal interesting reactivity in the single-electron activation of small molecules such as CO or diazo compounds.³¹ Isolation and characterization of these M^{II} complexes is challenging because of their inherent radical reactivity.

Scheme 4. Oxidation of Rh^{I} Complexes **7** and **8** to Form Stable Cationic Metalloradical Rh^{II} Analogues



Spurred by initial attempts to abstract the chloride ligand in **8** with Ag -salts, which resulted in an instantaneous color change from burgundy-red to blackish concomitant with formation of a Ag^0 -mirror rather than precipitation of anticipated AgCl , indicating redox-based reactivity, we observed smooth oxidation of both complex **7** and **8**¹⁸ with ferrocenium hexafluorophosphate to yield the one-electron oxidized $\text{PP}_3\text{Rh}^{\text{II}}\text{-Cl}$ complexes $[\mathbf{7}]\text{PF}_6$ and $[\mathbf{8}]\text{PF}_6$ (Scheme 4). Although not unprecedented,³² the isolation of stable $\text{Rh}^{\text{II}}\text{-chloro}$ complexes is unexpected because in other cases the presence of Cl^- has been reported to trigger disproportionation of otherwise stable Rh^{II} species.³³ In this case, disproportionation of $(\text{PP}_3)\text{Rh}^{\text{II}}\text{-Cl}$ is likely hindered by the strained (ligand) geometries of the hypothetical (trigonal pyramidal) $(\text{PP}_3)\text{Rh}^{\text{I}}$ and (constrained octahedral) $(\text{PP}_3)\text{Rh}^{\text{III}}\text{-Cl}$ products. Iridium complexes **9** and **10** could also be oxidized by ferrocenium hexafluorophosphate, but no stable Ir^{II} species could be isolated.

Electronic Absorption Spectra and TD-DFT Calculations.

The absorption spectra of **8** and $[\mathbf{8}]\text{PF}_6$ exhibit distinguishably different features (Figure 6). The parent compound exhibits bands at λ 475 nm (ϵ $3.6 \times 10^3 \text{ M}^{-1} \text{ cm}^{-1}$) and λ 528 nm (ϵ $2.7 \times 10^3 \text{ M}^{-1} \text{ cm}^{-1}$) in CH_2Cl_2 . For $[\mathbf{8}]\text{PF}_6$ only one absorption band at λ 550 nm (ϵ $2.5 \times 10^3 \text{ M}^{-1} \text{ cm}^{-1}$). Similar absorption spectra were obtained for complex **7** and its cation $[\mathbf{7}][\text{PF}_6]$ (see Supporting Information).

In an attempt to understand the nature of the electronic transitions we performed TD-DFT calculations with the Orca program at the *ri*-DFT BP86 level (COSMO CH_2Cl_2), using the Turbomole optimized geometries of **8** and $\mathbf{8}^+$. These correctly predict the experimentally observed red shifts and decreased intensities of the bands in the visible range of the spectra after oxidation of **8** to $\mathbf{8}^+$. The energies of the calculated transitions do not match the experimental data very accurately, with most of the calculated transitions occurring at roughly 100 nm (**8**) to 160 nm ($\mathbf{8}^+$) wavenumbers too high. This could perhaps be improved somewhat using a hybrid HF-DFT functional and a larger basis set, but the current data are sufficient for a qualitative understanding of the observed electronic transitions.

(28) For reviews on mononuclear Rh^{II} - and Ir^{II} -species, see: (a) DeWit, D. G. *Coord. Chem. Rev.* **1996**, *147*, 209–246. (b) Hettler, D. G. H.; Grützmacher, H.; Koekoek, A. J. J.; de Bruin, B. *Prog. Inorg. Chem.* **2007**, *55*, 247–354. (c) de Bruin, B.; Hettler, D. G. H. *Eur. J. Inorg. Chem.* **2007**, 211–230.

(29) de Bruin, B.; Budzelaar, P. H. M.; Gal, A. W. *Angew. Chem., Int. Ed.* **2004**, *43*, 4142–4157.

(30) (a) Davies, H. R. L.; Manning, J. R. *Nature* **2008**, *451*, 417–424. (b) Davies, H. R. L.; Hedley, S. J. *Chem. Soc. Rev.* **2007**, *36*, 1109–1119. (c) Merlic, C. A.; Zechman, A. L. *Synthesis* **2003**, 1137–1156.

(31) (a) Dzik, W. I.; Smits, J. M. M.; Reek, J. N. H.; de Bruin, B. *Organometallics* **2009**, *28*, 1631–1643. (b) Dzik, W. I.; Reek, J. N. H.; de Bruin, B. *Chem.—Eur. J.* **2008**, *14*, 7594–7599.

(32) Krumper, J. R.; Gerisch, M.; Suh, J. M.; Bergman, R. G.; Tilley, T. D. *J. Org. Chem.* **2003**, *68*, 9705.

(33) (a) Hettler, D. G. H.; Smits, J. M. M.; de Bruin, B. *Organometallics* **2004**, *23*, 4236–4246. (b) Sun, H.; Xue, F.; Nelson, A. P.; Redepenning, J.; DiMugno, S. G. *Inorg. Chem.* **2003**, *42*, 4507.

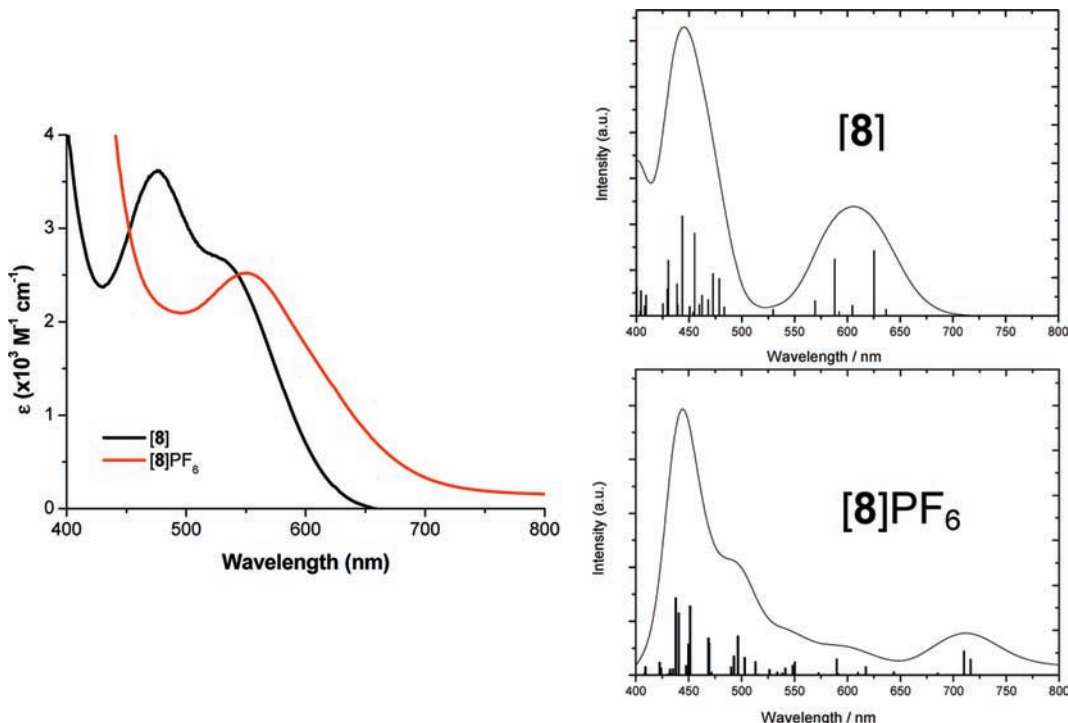


Figure 6. UV-vis spectra of complex **8** and **[8]PF₆** in CH₂Cl₂ (left), together with TD-DFT simulated spectra (right).

The lowest energy bands of Rh^I compound **8** (Exp: 528 nm, 475 nm; DFT: 625 nm, 588 nm) are transitions between (delocalized) MOs built mainly from σ -interactions between different metal d-orbitals and the lone pairs at the phosphorus ligand donors (HOMO \rightarrow LUMO and HOMO-1 \rightarrow LUMO), so these are basically “d-d transitions” with the P-lone pairs strongly (covalently) mixed in. The higher energy transitions (e.g., 454 nm in DFT; UV range in the experimental spectrum) are mainly $\pi \rightarrow \pi^*$ transitions. The lowest energy transitions of Rh^{II} compound **8**⁺ (Exp: 550 nm; DFT 710 nm, 716 nm) are transitions occurring between (delocalized) MOs built mainly from σ -interactions between different metal d-orbitals and the lone pairs at the phosphorus and chloro ligand (SOMO \rightarrow α -LUMO and β -HOMO-5 \rightarrow β -LUMO = SOMO), so again essentially “d-d transitions”, but with the phosphorus and chloride lone pairs strongly (covalently) mixed in. The higher energy transitions (i.e., the transitions between 650 and 450 nm in the DFT calculated spectrum) are dominated by mixed LMCT, MLCT, and π - π^* charge transfer bands (most of which are strongly mixed orbitals, involving linear combinations of several virtual orbitals of **8**⁺).

Electrochemistry. Cyclic voltammetry for complexes **7–10** was carried out to investigate the redox-chemistry of the electron-rich Rh^I and Ir^I complexes (Figure 7). As a reference complex the known species Rh(P(CH₂CH₂-PPh₂)₃)Cl⁹ [RhCl(**A**)], based on alkylphosphine ligand **A**, was chosen for comparison (Table 2). All complexes show (almost) fully reversible M^I/M^{II} oxidation waves at potentials ranging from -0.9 ([RhCl(**A**))] to -0.4 V (**8**), referenced vs Fc/Fc⁺. The relatively low potentials observed indicate facile oxidation, which likely results from the tetradentate coordination of four strongly electron-releasing phosphines, making the metal center electron-rich. Indeed, the oxidation potential is lowest for reference complex [RhCl(**A**)],⁹ containing one alkyl- and three

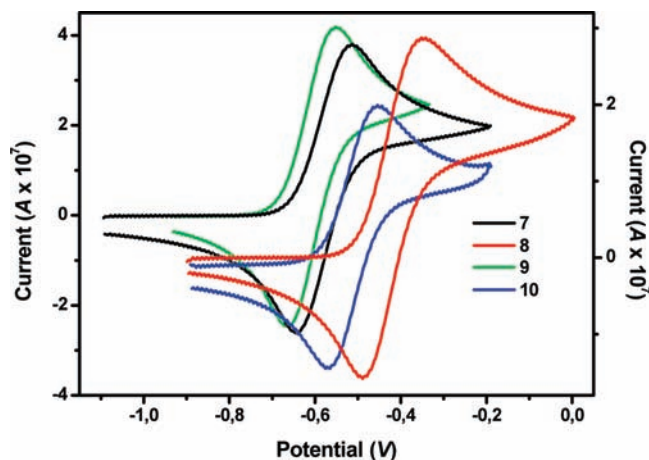


Figure 7. Cyclic voltammograms for complexes **7** (black line), **8** (red line), **9** (green lines), and **10** (blue line) in CH₂Cl₂ vs Fc/Fc⁺ using 0.1 mM *n*Bu₄PF₆, showing only the M^I/M^{II} oxidation/reduction potential. Scan rate $\nu = 0.1$ V s⁻¹.

Table 2. Cyclic Voltammetric Data for Complexes **7–10** and Reference Compound [RhCl(**A**)]^a

complex	$E_{1/2}$ (V)	ΔE (V)	I/I_0
7	-0.58	0.13	1.00
8	-0.42	0.13	0.85
9	-0.61	0.11	0.95
10	-0.51	0.12	0.97
[RhCl(A)] ⁹	-0.86	0.11	0.97

^a Referenced vs Fc/Fc⁺ using 0.1 mM *n*Bu₄PF₆, scan rate $\nu = 0.1$ V s⁻¹.

arylphosphine units, and highest for **8**, containing one arylphosphine and three phosphine amides.

The iridium complexes **9** and **10** show slightly lower oxidation potentials compared to their Rh-analogues (for **9**: $\Delta = 0.029$ V; for **10**: $\Delta = 0.090$ V), which is in accord

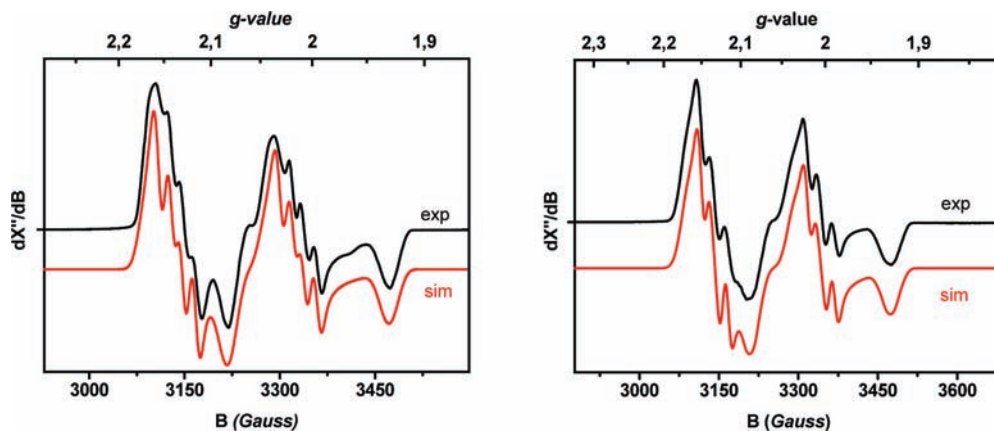


Figure 8. Experimental (black) and simulated (red) X-band EPR spectra of [7]PF₆ (left) and [8]PF₆ (right)¹⁸ in frozen acetone. TBAH (~0.1 M) was added to obtain a better glass. Experimental details for [7]PF₆: 40K, frequency 9.3807 GHz, microwave power 0.2 mW, modulation amplitude 2 G. Experimental details for [8]PF₆: 20K, frequency 9.3794 GHz, microwave power 0.2 mW, modulation amplitude 4 G. The simulation parameters are listed in Table 3.

with previous observations.²⁸ As expected, solution-state RT magnetization measurements by Evans' method³⁴ are consistent with the formulation of complexes [7]PF₆ and [8]PF₆ as radical species, with μ_{eff} values of 2.06(3) μ_{B} ([7]PF₆) and 2.29(1) μ_{B} ([8]PF₆). These values are somewhat larger than the spin-only values (1.73 μ_{B}), thus indicating spin-orbit influences, and they are in the same range as PNP-based mononuclear Rh^{II} species reported by Milstein and co-workers.³⁵ The solution phase Evans' method is not very accurate, and the obtained values are somewhat overestimated. RT susceptibility values obtained in the solid state (Evans balance) for related NNN-based Rh^{II} complexes³⁶ are somewhat smaller (in the range 1.6–1.95 μ_{B}), and the X-band electron paramagnetic resonance (EPR) spectra of [7]PF₆ and [8]PF₆ indeed reveal small orbital contributions to the magnetic susceptibility.

EPR Spectroscopic Analysis and DFT Calculations of Metalloradical Species. The X-band EPR spectra of [7]PF₆ and [8]PF₆¹⁸ are shown in Figure 8. Identical data were obtained for stored (one-month old) and in situ generated samples, indicative of highly stable radical species. The EPR parameters of the DFT optimized geometries of both 7⁺ and 8⁺ were also calculated (BP86, TZP). Simulation of the experimental EPR spectra of [7]PF₆ (20 K) and [8]PF₆ (40 K) reveal rhombic *g*-tensors with moderate *g*-anisotropy and resolved superhyperfine couplings with mainly three P atoms; large coupling with P₂ and smaller couplings with P₃ and P₄ (Table 2). The fourth P-atom (pivotal P₁) and Rh show no resolved hyperfine couplings.

Interestingly, the corresponding in situ oxidized Ir-complexes did not reveal any EPR-signals. This could mean that the Ir^{II} species are inherently unstable (only detectable on the fast CV time scale), but its EPR silence could also be due to very fast relaxation caused by the

presence of many close-lying excited states, as has been observed for Ir^{II}(por) species.³⁷

The experimentally derived EPR parameters are in reasonable agreement with those calculated with DFT (see Table 3), and thus the geometries of 7⁺ and 8⁺ in frozen solution should be very close to the DFT optimized structures, which in turn should resemble those present in the solid state, as was established for the X-ray structure of 8⁺ (see Supporting Information). A distorted geometry in-between a trigonal bipyramid (tbp) and a square pyramid (sqpy) is revealed. This is quite remarkable, because five-coordinate Rh^{II}-complexes generally adopt a square-pyramidal geometry (Jahn–Teller effect).^{34b}

The geometry of 8⁺, both in the solid and in (frozen) solution, is thus best described as distorted square pyramidal (sqpy), with the pivotal P donor (P₁), the chloro ligand, and two of the side arm P donors (P₃ and P₄) in the square plane and the third side arm P donor at the apical position (P₂). However, this geometry is strongly distorted from the ideal sqpy geometry toward a tbp, because the ligand is preshaped to form the latter and therefore does not accommodate the appropriate angles for a sqpy. The complex thus adopts a distorted geometry in-between the geometries preferred by either ligand and metal. On the basis of the similarity of the EPR spectra (Figure 8, Table 3), 7⁺ should have a similar coordination geometry.

Because of its distorted geometry, the DFT spin-carrying orbital (singly occupied molecular orbital, SOMO) of 8⁺ is not the expected metal *d*_{z²} orbital normally encountered in sqpy *d*⁷ complexes (*d*_{xz}+*d*_{yz}⁴, *d*_{xy}², *d*_{z²}¹, *d*_{x²-y²}⁰ configuration), but a strongly delocalized orbital constructed of a different Rh *d*-orbital (possibly the “*d*_{xy}” or “*d*_{x²-y²}”), in bonding combination with lone pairs of two side arm P donors. The rather small *g*-anisotropy excludes a (weakly distorted) tbp complex (*d*_{xz}+*d*_{yz}⁴, *d*_{xy}+*d*_{x²-y²}³, *d*_{z²}¹, *d*_{z²}⁰ configuration), because (close to) degenerate *d*_{xy} and *d*_{x²-y²} orbitals should lead to a much larger *g*-anisotropy (*g*_{zz} ≫ *g*_e).^{28b} The distorted geometry actually leads to strong mixing of the *d*-orbitals among several of the lower and higher lying orbitals, which prevents a proper assignment of the “*d*-orbital configuration”

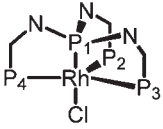
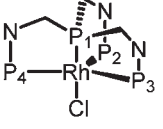
(34) Evans, D. F. *J. Chem. Soc.* **1959**, 2003–2005.

(35) Feller, M.; Ben-Ari, E.; Gupta, T.; Shimon, L. J. W.; Leitus, G.; Diskin-Posner, Y.; Weiner, L.; Milstein, D. *Inorg. Chem.* **2007**, *46*, 10479–10490.

(36) See ref 28 and: Hetterscheld, D. G. H.; Klop, M.; Kicken, R. J. N. A. M.; Smits, J. M. M.; Reijerse, E. J.; de Bruin, B. *Chem.—Eur. J.* **2007**, *13*, 3386–3405.

(37) Zhai, H.; Bunn, A.; Wayland, B. B. *Chem. Commun.* **2001**, 1294–1295.

Table 3. Experimental and DFT Calculated g -Values, Hyperfine Coupling Constants, A [MHz], and Spin Populations ρ of [7]PF₆ and [8]PF₆^a

 7 ⁺				
g -values	Exp.	$g_{11} = 2.089$	$g_{22} = 2.070$	$g_{33} = 2.002$
	<i>comp.</i>	<i>$g_{11} = 2.090$</i>	<i>$g_{22} = 2.058$</i>	<i>$g_{33} = 1.997$</i>
A-tensors	ρ	A_{11}	A_{22}	A_{33}
³¹ P ₂ exp.	-	600	600	750
<i>comp.</i>	25%	464	467	627
³¹ P ₃ exp.	-	80	110	NR
<i>comp.</i>	7%	60	62	103
³¹ P ₄ exp.	-	NR	60	NR
<i>comp.</i>	3%	16	19	38
³¹ P ₁ exp.	-	NR	NR	NR
<i>comp.</i>	-1%	-11	-10	-8
¹⁰³ Rh exp.	-	NR	NR	NR
<i>comp.</i>	50%	31	11	-29
 8 ⁺				
g -values	Exp.	$g_{11} = 2.092$	$g_{22} = 2.067$	$g_{33} = 2.005$
	<i>comp.</i>	<i>$g_{11} = 2.085$</i>	<i>$g_{22} = 2.064$</i>	<i>$g_{33} = 1.996$</i>
A-tensors	ρ	A_{11}	A_{22}	A_{33}
³¹ P ₂ exp.	-	585	580	740
<i>comp.</i>	24%	493	494	646
³¹ P ₃ exp.	-	70	90	NR
<i>comp.</i>	6%	67	68	99
³¹ P ₄ exp.	-	NR	60	NR
<i>comp.</i>	3%	23	27	46
³¹ P ₁ exp.	-	NR	NR	NR
<i>comp.</i>	0.4%	-9	-8	-4
¹⁰³ Rh exp.	-	NR	NR	NR
<i>comp.</i>	51%	23	9	-37

^a DFT values are given in italics. NR = not resolved. The experimental values are least-square "best fit" values obtained by simulation of the experimental X-band EPR spectra.

of 8⁺ on the basis of the DFT calculations. For both 7⁺ and 8⁺, about 50% of the DFT spin density resides on Rh and about 25% on the "apical" P₂-donor (Figure 9, Table 3). The species are thus best described as strongly covalent radicals. They have substantial metallo-radical character, but with a strong contribution of the sqpy "axial" P₂ donor.

Reactivity of Metallo-radicals toward Activation of H₂. We previously reported on the remarkable capability of [8]PF₆ to activate H₂.¹⁸ When this complex was exposed to molecular hydrogen for 24 h (5 bar, CD₂Cl₂), Rh^{III}H species [Rh(3)(H)Cl]PF₆ was formed quantitatively in what appeared to be a direct oxidation-reaction to split H₂ into two protons and two electrons with subsequent recombination. We thus wondered if the linkage isomeric compound [7]PF₆, showing subtly different redox-behavior, would demonstrate similar reactivity (Scheme 5). Indeed, dihydrogen activation takes place but at lower rates than with [8]PF₆ under identical conditions. Full conversion toward [Rh(1)(H)Cl]PF₆ (**13**) is achieved after 6 days instead of 24 h. Complex [7]PF₆ shows a lower reduction potential (at -0.58 V for the Rh^I/Rh^{II} couple) compared to [8]PF₆ (-0.42 V) (see Figure 7 and Table 2). Hence, the redox-potential of [7]PF₆ vs NHE is only 0.12 V vs 0.28 V for [8]PF₆.¹⁸ These values imply that the overall oxidation of H₂ to 2H⁺, which is thermodynamically allowed (even without subsequent metal protonation), should indeed be possible. Furthermore, it provides a rationale for the observed slower reaction with complex [7]PF₆, as it shows a lower overpotential. We postulate an outer-sphere redox-reaction involving full oxidation of H₂ and consecutive protonation of the generated Rh^I-complex. The difference in rate supports our proposed mechanism in which dihydrogen is fully reduced by the metallo-radical complex over alternative mechanisms such as discussed by Rauchfuss and co-workers, involving oxidative deprotonation of an Ir(H₂) fragment with a non-innocent ligand radical,³⁸ or via homolytic H₂ bond cleavage in a trimolecular process, analogous to reported Rh^{II}(por) or Co(CN)₅³⁻ systems.³⁹ Given the very sterically encumbered nature of the ligand and the resulting pseudoencapsulation of the metal center, the latter mechanism seems very unlikely.

In the ³¹P NMR spectrum of **13** an AM₂X spin pattern could be discerned while the ¹H NMR spectrum showed a complex doublet-of-doublet-of-doublet-of-triplets at δ -6.49 ppm, with a large ²J_{P-H} coupling of 167.6 Hz. The hydrido ligand is *trans* to one of the side arm P-atoms and the chloro ligand *trans* to the pivotal P donor. Independent synthesis of analogous salts of **13** confirmed the above assignment.⁴⁰

Initial attempts to further utilize the radical character of the Rh^{II} complexes 7⁺ or 8⁺ have so far not been

(38) Another pathway for H₂ activation was recently reported, see: Ringenberg, M. R.; Latha Kokatam, S.; Heiden, Z. M.; Rauchfuss, T. B. *J. Am. Chem. Soc.* **2008**, *130*, 788–789.

(39) H₂ activation by Rh^{II}-porphyrins and Rh^{II}-salen complexes is well-documented, see: (a) Cui, W.; Wayland, B. B. *J. Am. Chem. Soc.* **2004**, *126*, 8266–8274. (b) Zhang, X. X.; Wayland, B. B. *J. Am. Chem. Soc.* **1994**, *116*, 7897–7898. (c) Bunn, A. G.; Wei, M.; Wayland, B. B. *Organometallics* **1994**, *13*, 3390–3392. (d) Wayland, B. B.; Ba, S.; Sherry, A. E. *Inorg. Chem.* **1992**, *31*, 148–150. (e) James, B. R.; Stynes, D. V. *J. Am. Chem. Soc.* **1972**, *94*, 6225–6226.

(40) Similar Rh^{III} species have been made via classic routes, e.g., from complex [Rh(A)Cl], see ref 9. For the related tris(indolylphosphino)methane ligand reported by Lahuerta, see ref 6a.

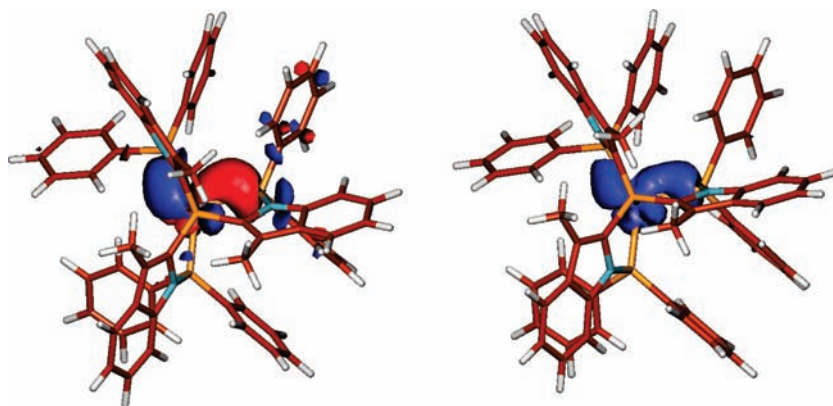
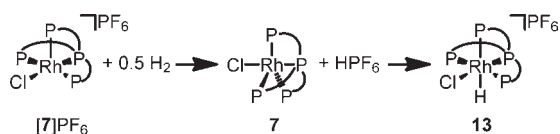


Figure 9. SOMO (left) and spin density (right) of complex 8^+ (view along the Cl–Rh–P₁ axis). Plots for 7^+ are similar.

Scheme 5. Formation of Cationic Rh^{III}(H)Cl-Species **13** via Oxidation of H₂ by [7]PF₆, and Subsequent Protonation of the Rh^I Species



successful. We have investigated possibilities to apply the observed activation of dihydrogen in hydrogen atom-transfer reactions, using the Rh^{II} metalloradicals based on these novel and modular tripodal phosphorus ligands as mediators or initiators. No reaction was observed with the H-atom transfer⁴¹ (HAT) donor 9,10-dihydroanthracene or with TEMPO as a HAT-acceptor reagent. We will intensify these efforts, coupled with strategies to modulate the periphery of our tripodal ligand system to enhance reactivity.

Conclusions

Summarizing, we have reported the straightforward synthesis of three novel tripodal, potentially tetradentate phosphorus ligands **1–3**, derived from 3-methylindole as building block. The corresponding Cu^ICl-complexes **4–6** display coordination of only three phosphorus atoms and give a 7:3 *trans/cis* selectivity in the cyclopropanation of styrene with EDA. However, the complementary, linkage isomeric PP₃ frameworks enforce C₃-symmetry onto neutral M^I complexes **7–10** (M = Rh, Ir), as deduced from NMR spectroscopic and X-ray crystallographic data. Cationic Rh^I complexes were obtained with nbd (**11**) and CO (**12**) as a co-ligand. Norbornadiene complex **11** displays monodentate coordination of the diene ligand, which is hitherto unprecedented, to the best of our knowledge. Cyclic voltammetry on the chloride complexes **7–10** showed facile oxidation to the corresponding M^{II} species and a strong dependence of the oxidation potential on the overall ligand structure. Reference compound [RhCl(A)], which features a more flexible and electron-rich aliphatic PP₃ scaffold, proved significantly easier to oxidize. Hence, the inherent, designed rigidity built-in for ligand **1** and **3** has a strong governing influence

on the overall structure and its reactivity. The Rh^{II}-complexes were characterized by EPR-spectroscopy and for complex [8]PF₆ also by X-ray crystallography. The pronounced overall C₃-symmetry dictated by the very rigid ligand geometry was also preserved in this corresponding oxidation product.

The isolated metalloradical complexes 7^+ and 8^+ are rare Rh^{II}Cl compounds with an unusual coordination geometry in between a trigonal bipyramid and a square pyramid. These species appear bench-stable as solids, and they also do not show appreciable decomposition in common solvents, indicating highly effective shielding of the Rh^{II} center by the ligand sphere. Notwithstanding this, both 7^+ and 8^+ react with molecular hydrogen to quantitatively form the corresponding cationic Rh^{III} hydrido-chloride complexes. The slower reaction with 7^+ , which has a lower oxidation potential compared to 8^+ ($\Delta = 0.16$ V), further supports the proposed mechanism via complete outer-sphere oxidation of molecular hydrogen to protons. Further studies aimed at the reactivity of these unusual Rh^{II} metallo-radicals are ongoing, including studies derived from the related cationic Rh^I species.

This detailed study of the coordination properties of the novel PP₃ frameworks **1–3** illustrates that indeed unusual geometries of metal complexes as well as novel reactivity of these complexes can be achieved. This is the result of the highly rigid nature of the ligands in conjunction with the encapsulating effect of the tripodal coordination mode, which concurrently stabilize reactive species and direct their reactivity. It is remarkable to observe that these rigid PP₃ ligands can accommodate tetradentate complexation to Rh in *three* oxidation states (Figure 10), with subtle but distinct differences in the overall structure. This concept will be further expanded on for further reactivity studies, including with other metals as well. Also the activation of small molecules other than H₂ will be targeted, including N₂ and NH₃.⁴²

Experimental Section

General Procedures. All reactions were carried out under an atmosphere of argon using standard Schlenk techniques. With exception of the compounds given below, all reagents were purchased from commercial suppliers and used without further purification. Diphenyl(3-methyl-2-indolyl)phosphine,¹⁴ tris-2-(3-methylindolyl)phosphine⁴³ and RhCl(P(CH₂CH₂PPh₂)₃)^{9a}

(41) (a) Wu, A.; Masland, J.; Swartz, R. D.; Kaminsky, W.; Mayer, J. M. *Inorg. Chem.* **2007**, *46*, 11190, and references therein. (b) Büttner, T.; Geier, J.; Frison, G.; Harmer, J.; Calle, C.; Schweiger, A.; Schönberg, H.; Grützmaier, H. *Science* **2005**, *307*, 235–238.

(42) van der Vlugt, J. I. *Chem. Soc. Rev.* **2010**, *39*, 2302–2322.

(43) This compound has been synthesized before using an amination protecting route, see ref 15.

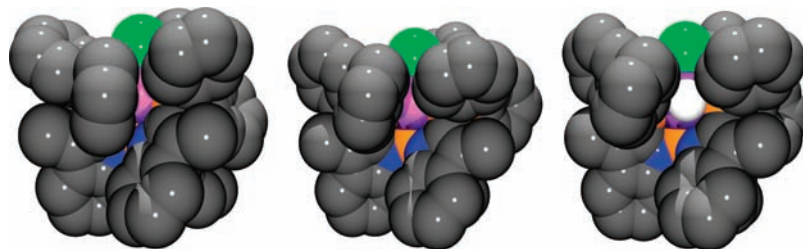


Figure 10. Space-filling models for complexes **7** (left), **[7]PF₆** (middle), and **13** (right), showing the very sterically encumbered but subtly changing situation around the respective Rh^I, Rh^{II}, and Rh^{III}-center, respectively. Complex **7** has been crystallographically characterized (see Supporting Information), whereas **[7]PF₆** and **13** have been calculated by DFT.

were synthesized according to published procedures. THF, pentane, hexane and diethyl ether were distilled from sodium benzophenone ketyl; CH₂Cl₂, isopropanol, and methanol were distilled from CaH₂, and toluene was distilled from sodium under nitrogen. Melting points were recorded on a Gallenkamp melting point apparatus and are uncorrected. NMR spectra (¹H, ³¹P and ¹³C) were measured on a Varian INOVA 500 MHz or a Varian MERCURY 300 MHz. High resolution mass spectra were recorded on a JEOL JMS SX/SX102A four sector mass spectrometer; for FAB-MS 3-nitrobenzyl alcohol was used as matrix. Elemental analyses were carried out at Kolbe Mikroanalytisches Laboratorium in Mülheim an der Ruhr. Cyclic voltammograms were recorded on an Eco Chemie Autolab PGSTAT10 potentiostat. UV–vis spectra were measured on a Hewlett-Packard 8453 spectrophotometer. X-band EPR spectroscopy measurements were performed with a Bruker EMX Plus spectrometer.

Tris-*N*-(3-methyl-2-diphenylphosphinoindolyl)phosphine (1).¹⁷ To a solution of diphenyl(3-methyl-2-indolyl)phosphine (4.0 g, 12.7 mmol) in THF (60 mL) was added *n*-BuLi (2.5 M in hexanes, 5.08 mL, 12.7 mmol) at -78°C . The resulting solution was stirred for 30 min and phosphorus trichloride (369 μL , 4.2 mmol) was added. The reaction mixture was stirred for 2 days allowing to warm to rt. The resulting white suspension was concentrated in vacuo and redissolved in CHCl₃ (50 mL). The suspension was filtered through a pad of SiO₂, which was rinsed with CHCl₃ (2 \times 50 mL). The solvent was removed under reduced pressure and the resulting white solid was washed with Et₂O (3 \times 20 mL) and dried in vacuo. Yield: 3.21 g (78%). Mp = 293 $^{\circ}\text{C}$ (dec.). ¹H NMR (500 MHz; CDCl₃; 298 K): δ 7.54 (d, J = 7.8 Hz, 3H), 7.28–7.26 (m, 3H), 7.19–7.14 (m, 9H), 7.11 (t, J = 7.6 Hz, 6H), 7.07–7.04 (m, 3H), 7.02–6.96 (m, 9H), 6.66 (d, J = 8.5 Hz, 3H), 6.51 (t, J = 7.2 Hz, 6H), 1.77 (s, 9H). ¹³C NMR (126 MHz; CDCl₃; 298 K): δ 134.2 (d, J_{CP} = 20.6 Hz), 133.8 (d, J_{CP} = 30.9 Hz), 133.6–133.2 (m), 131.4 (d, J_{CP} = 18.1 Hz), 128.4 (d, J_{CP} = 13.2 Hz), 128.3–127.9 (m), 127.2, 125.8 (m), 124.9, 120.8, 119.4, 114.0, 10.7 (CH₃). ³¹P{¹H}-NMR (202 MHz; CDCl₃; 298 K): δ 73.72 (q, J = 197.3 Hz, 1P), –29.58 (d, J = 197.4 Hz, 3P). Anal. Calcd for C₆₃H₅₁N₃P₄ (%): C 77.69, H 5.28, N 4.31; found: C 77.41, H 5.47, N 4.22. HRMS (FAB) calcd for [M + H]⁺ C₆₃H₅₂N₃P₄, 974.3112; found, 974.3117.

Tris-*N*-(3-methyl-2-diisopropylphosphinoindolyl)phosphine (2). To a solution of diisopropyl(3-methyl-2-indolyl)phosphine (0.51 g, 2.1 mmol) in THF (10 mL) was added *n*-BuLi (2.5 M in hexanes, 0.83 mL, 2.1 mmol) at -78°C . The resulting solution was stirred for 30 min, and phosphorus trichloride (369 μL , 4.2 mmol) was added. The reaction mixture was stirred overnight allowing to warm to rt. The resulting solution was concentrated in vacuo, and the off-white residue was purified by flash SiO₂ chromatography (3% EtOAc in hexanes). Yield: 0.36 g (68%). ¹H NMR (500 MHz; CDCl₃; 298 K): δ 7.49 (d, J = 7.7 Hz, 3H), 6.99 (t, J = 7.4 Hz, 3H), 6.69 (t, J = 7.4 Hz, 3H), 6.35 (d, J = 8.5 Hz, 3H), 2.48–2.43 (br m, 3H), 2.39 (s, 9H), 2.23–2.19 (br m, 3H), 1.24 (dd, J = 15.7, 6.9 Hz, 18H), 0.77 (dd, J = 17.2, 6.8 Hz, 9H), –0.06 (dd, J = 13.3, 6.8 Hz, 9H) ppm. ³¹P{¹H}-NMR (202 MHz; CDCl₃; 298 K): δ 67.27 (q, J = 219.5 Hz, 1P), –9.92 (d, J = 219.3 Hz, 3P) ppm.

Tris-2-(3-methyl-*N*-diphenylphosphinoindolyl)phosphine (3).

To a solution of tris-2-(3-methylindolyl)phosphine (1.5 g, 3.56 mmol) in THF (50 mL) was added *n*-BuLi (2.5 M in hexanes, 4.28 mL, 10.7 mmol) at -78°C . The resulting solution was stirred for 1 h, and chlorodiphenylphosphine (1.92 mL, 10.7 mmol) was added. The reaction mixture was stirred for 16 h allowing to warm slowly to rt. The resulting white suspension was concentrated in vacuo and redissolved in CHCl₃ (40 mL). The suspension was filtered through a pad of basic alumina, which was rinsed with CHCl₃ (2 \times 20 mL). The solvent was removed under reduced pressure, and the resulting white solid was washed with Et₂O (3 \times 10 mL) and dried in vacuo. Yield: 2.00 g (58%). Mp = 267 $^{\circ}\text{C}$ (dec.). ¹H NMR (500 MHz; CDCl₃, 298 K): δ 7.43 (d, J = 7.9 Hz, 3H), 7.24–7.10 (m, 30H), 7.02 (t, J = 7.4 Hz, 3H), 6.83 (t, J = 7.7 Hz, 3H), 6.71 (d, J = 8.3 Hz, 3H), 2.05 (s, 9H). ¹³C NMR (126 MHz; CDCl₃, 298 K): δ 140.6 (d, J_{CP} = 10.7 Hz), 136.4–136.2 (m), 136.1 (d, J_{CP} = 16.8 Hz), 133.8–133.7 (m), 131.9 (t, J_{CP} = 21.1 Hz), 128.8, 128.3 (t, J_{CP} = 5.5 Hz), 124.3–124.2 (m), 122.4, 120.0, 118.9, 114.5, 9.8 (CH₃). ³¹P{¹H}-NMR (202 MHz; CDCl₃, 298 K): δ 37.27 (d, J = 159.2 Hz, 3P), –75.07 (q, J = 159.3 Hz, 1P). Anal. Calcd for the triphosphine oxide C₆₃H₅₁N₃O₃P₄ (%): C 74.04, H 5.03, N 4.11; found: C 74.20, H 5.17, N 4.12. HRMS (FAB) calcd for [M + H]⁺ C₆₃H₅₂N₃P₄, 974.3112; found, 974.3108.

[Cu(1)Cl] (4). Tetraphosphine **1** (150 mg, 0.15 mmol) and [CuCl(cod)]₂ (32 mg, 0.08 mmol) are stirred in CH₂Cl₂ (8 mL) for 1 h at rt. The resulting pale yellow solution was concentrated under reduced pressure, and hexanes (10 mL) were added to precipitate a pale yellow solid. The solid was collected by filtration and washed with hexanes (5 mL). Crystals suitable for X-ray single crystal diffraction were obtained by slow diffusion of toluene in a CH₂Cl₂ solution at rt. Yield: 128 mg (77%). ¹H NMR (500 MHz; CD₂Cl₂; 298 K): δ 7.33 (m, 9H), 7.30 (d, J = 7.2 Hz, 9H), 7.22 (s, 6H), 7.10 (t, J = 7.3 Hz, 3H), 6.97 (q, J = 7.7 Hz, 9H), 6.70 (t, J = 7.8 Hz, 3H), 6.28 (d, J = 8.5 Hz, 3H), 1.56 (s, 9H) ppm. ¹³C NMR (126 MHz; CD₂Cl₂, 298 K): δ 140.6 (dd, J_{CP} = 7.7, 2.0 Hz, C_q), 133.7–133.5 (m), 133.4–133.3 (m), 131.0 (br m, C_q), 129.4, 129.3, 128.6–128.3 (m), 127.3 (d, J_{CP} = 2.9 Hz, C_q), 125.1, 122.0, 119.7, 114.70, 10.32 (CH₃) ppm. ³¹P{¹H}-NMR (202 MHz; CD₂Cl₂; 298 K): δ 58.70 (br q, J = 195.9 Hz, 1P), –27.68 (br d, J = 197.6 Hz, 3P) ppm.

[Cu(2)Cl] (5). Tetraphosphine **2** (50 mg, 0.065 mmol) and [CuCl(cod)]₂ (12 mg, 0.028 mmol) are stirred in CH₂Cl₂ (2 mL) for 1 h at rt. The resulting pale yellow solution was concentrated under reduced pressure, and hexanes (10 mL) were added to precipitate a pale yellow solid. The solid was collected by filtration and washed with hexanes (5 mL). Crystals suitable for X-ray single crystal diffraction were obtained by slow diffusion of hexane in a CH₂Cl₂ solution at rt. Yield: 18 mg (37%). ¹H NMR (300 MHz; CD₂Cl₂; 298 K): δ 7.57 (d, J = 8.1 Hz, 3H), 7.09 (t, J = 7.4 Hz, 3H), 6.72 (t, J = 7.8 Hz, 3H), 6.01 (br d, J = 8.4 Hz, 3H), 2.89 (br s, 3H), 2.47 (s), 1.95 (quintuplet, J = 7.1 Hz, 3H), 1.43–1.24 (m, 18H), 0.75–0.57 (m, 18H) ppm. ³¹P{¹H}-NMR (121.5 MHz; CD₂Cl₂; 298 K): δ 59.27 (q, J = 172.2 Hz, 1P), –2.32 (d, J = 173.7 Hz, 3P) ppm.

[Cu(3)Cl] (6). Tetraphosphine **3** (153 mg, 0.16 mmol) and [CuCl(cod)]₂ (33 mg, 0.08 mmol) are stirred in CH₂Cl₂ (8 mL) for 1 h at rt. The resulting yellow solution was concentrated under reduced pressure and hexanes (10 mL) were added to precipitate a yellow solid. The solid was collected by filtration and washed with hexanes (5 mL). Crystals suitable for X-ray single crystal diffraction were obtained by slow diffusion of hexane in a CH₂Cl₂ solution at rt. Yield: 165 mg (98%). ¹H NMR (500 MHz; CD₂Cl₂; 298 K): δ 7.37–7.28 (m, 21H), 7.15 (br m, 12H), 7.01 (t, *J* = 7.5 Hz, 3H), 6.85 (t, *J* = 7.6 Hz, 3H), 6.76 (d, *J* = 8.4 Hz, 3H), 1.96 (s, 9H) ppm. ¹³C NMR (126 MHz; CD₂Cl₂, 298 K): δ 140.7 (C_q), 134.3 (d, *J*_{CP} = 6.3 Hz, C_q), 132.9 (br, C_q), 132.5 (br), 130.0 (br), 128.6 (br), 125.8 (C_q), 123.9, 121.2, 120.0, 115.3, 10.9 (CH₃) ppm. ³¹P NMR (202 MHz; CD₂Cl₂): δ 40.30 (br d, *J*_{PP} = 119.7 Hz, 3P), –63.55 (br m, 1P) ppm.

[Rh(1)Cl] (7).¹⁷ Tetraphosphine **1** (800 mg, 0.82 mmol) and [Rh(cod)Cl]₂ (203 mg, 0.41 mmol) are stirred in CH₂Cl₂ (40 mL) for 0.5 h at rt. The resulting deep red solution was concentrated under reduced pressure, and hexanes (100 mL) were added to precipitate a dark red solid. The solid was collected by filtration and washed with hexanes (20 mL). Crystals suitable for X-ray single crystal diffraction were obtained by slow diffusion of hexane in a THF solution at rt. Yield: 834 mg (91%). Mp = 319 °C. ¹H NMR (500 MHz; CDCl₃; 298 K): δ 7.46 (d, *J* = 7.9 Hz, 3H), 7.29 (br s, 6H), 7.22 (t, *J* = 7.3 Hz, 3H), 7.18 (t, *J* = 7.6 Hz, 3H), 7.10 (t, *J* = 7.5 Hz, 12H), 7.04 (t, *J* = 7.3 Hz, 3H), 6.98 (t, *J* = 7.8 Hz, 3H), 6.83 (t, *J* = 7.6 Hz, 6H), 6.70 (d, *J* = 8.4 Hz, 3H), 1.59 (s, 9H). ¹³C NMR (126 MHz; CDCl₃; 298 K): δ 139.4 (m), 136.1 (m), 134.2–133.9 (m), 130.8–130.5 (m), 128.9 (m), 128.5, 128.2 (m), 127.9, 125.3, 122.1, 120.5, 113.8, 10.3 (CH₃). ³¹P{¹H}-NMR (202 MHz; CDCl₃; 298 K): δ 131.75 (dq, *J*_{PRh} = 169.7 Hz, *J*_{PP} = 30.3 Hz, 1P), 5.74 (dd, *J*_{PRh} = 138.0 Hz, *J*_{PP} = 30.2 Hz, 3P). Anal. Calcd for the CH₂Cl₂ adduct C₆₄H₅₃Cl₃N₃P₄Rh (%): C 64.20, H 4.46, N 3.51; found: C 64.19, H 4.55, N 3.41. HRMS (FAB) calcd for [M + H]⁺ C₆₃H₅₂Cl₃N₃P₄Rh, 1112.1855; found, 1112.1849.

[Rh(1)Cl]PF₆ ([7]PF₆). Complex **7** (80 mg, 0.072 mmol) and ferrocenium hexafluorophosphate (24 mg, 0.072 mmol) are stirred in CH₂Cl₂ (4 mL) for 1 h at rt. The resulting deep purple solution was concentrated under reduced pressure. The dark purple residue was washed with Et₂O (3 × 10 mL) and dried in vacuo. Yield: 77 mg (85%). Mp = 190 °C. Anal. Calcd for the CH₂Cl₂ adduct C₆₄H₅₃Cl₃F₆N₃P₅Rh (%): C 57.27, H 3.98, N 3.13; found: C 57.32, H 4.68, N 3.01. HRMS (FAB) calcd for [M – PF₆]⁺ C₆₃H₅₁Cl₃N₃P₄Rh, 1111.1777; found, 1111.1786.

[Rh(3)Cl] (8).¹⁸ Tetraphosphine **3** (400 mg, 0.41 mmol) and [Rh(cod)Cl]₂ (101 mg, 0.21 mmol) are stirred in CH₂Cl₂ (20 mL) for 0.5 h at rt. The resulting deep red solution was concentrated under reduced pressure and hexanes (40 mL) were added to precipitate a burgundy-colored solid. The solid was collected by filtration and washed with hexanes (2 × 10 mL). Crystals suitable for X-ray single crystal diffraction were obtained by slow diffusion of hexane in a CH₂Cl₂ solution at rt. Yield: 378 mg (83%). Mp = 303 °C (dec.). ¹H NMR (500 MHz; CDCl₃; 298 K): δ 7.55 (d, *J* = 8.0 Hz, 3H), 7.05–7.02 (m, 15H), 6.82–6.77 (m, 21H), 6.42 (d, *J* = 8.5 Hz, 3H), 2.55 (s, 9H). ¹³C NMR (126 MHz; CDCl₃; 298 K): δ 139.7–139.6 (m), 136.8–136.7 (m), 136.1 (d, *J*_{CP} = 8.7 Hz), 129.8 (m), 128.1 (d, *J*_{CP} = 4.9 Hz), 124.1, 122.3 (m), 121.0, 120.3, 116.3, 10.5 (CH₃). ³¹P{¹H}-NMR (202 MHz; CDCl₃; 298 K): δ 73.95 (dd, *J*_{PRh} = 158.8 Hz, *J*_{PP} = 26.9 Hz, 3P), 43.49 (dq, *J*_{PRh} = 108.2 Hz, *J*_{PP} = 26.8 Hz, 1P). Anal. Calcd for the CH₂Cl₂ adduct C₆₄H₅₃Cl₃N₃P₄Rh (%): C 64.20, H 4.46, N 3.51; found: C 64.22, H 4.51, N 3.48. HRMS (FAB) calcd for [M]⁺ C₆₃H₅₁Cl₃N₃P₄Rh, 1111.1777; found, 1111.1771.

[Rh(3)Cl]PF₆ ([8]PF₆).¹⁸ Complex **8** (100 mg, 0.09 mmol) and ferrocenium hexafluorophosphate (30 mg, 0.09 mmol) are stirred in CH₂Cl₂ (5 mL) for 1 h at rt. The resulting deep purple solution was concentrated under reduced pressure. The dark purple residue was washed with Et₂O (3 × 10 mL) and dried in vacuo. Crystals suitable for X-ray single crystal diffraction were

obtained by slow diffusion of hexane in a CH₂Cl₂ solution at rt. Yield: 54 mg (48%). Mp = 220 °C. Anal. Calcd for the CH₂Cl₂ adduct C₆₄H₅₃Cl₃F₆N₃P₅Rh (%): C 57.27, H 3.98, N 3.13; found: C 57.88, H 4.06, N 3.24. HRMS (FAB) calcd for [M – PF₆]⁺ C₆₃H₅₁Cl₃N₃P₄Rh, 1111.1777; found, 1111.1777.

[Ir(1)Cl] (9). Tetraphosphine **1** (100 mg, 0.10 mmol) and [Ir(cod)Cl]₂ (35 mg, 0.05 mmol) are stirred in CH₂Cl₂ (4 mL) for 1 h at rt. The resulting orange solution was filtered through Celite and concentrated under reduced pressure. The solid was washed with hot EtOH (10 mL) and dried in vacuo. Yield: 78 mg (65%). Mp = 224 °C (dec.). ¹H NMR (500 MHz; CD₂Cl₂; 298 K): δ 7.50 (d, *J* = 7.8 Hz, 3H), 7.21 (t, *J* = 7.4 Hz, 6H), 7.11–6.93 (m, 30H), 6.87 (d, *J* = 8.4 Hz, 3H), 1.63 (s, 9H). ¹³C NMR (126 MHz; CD₂Cl₂, 298 K): δ 138.8–138.7 (m), 134.5 (m), 133.82, 133.6 (m), 131.6–131.4 (m), 129.0, 128.8–128.6 (m), 128.3–128.2 (m), 128.1–127.7 (m), 125.3, 122.5–122.4 (m), 121.2–121.0 (m), 114.4 (m), 10.7 (CH₃). ³¹P{¹H}-NMR (202 MHz; CD₂Cl₂; 298 K): δ 93.15 (q, *J*_{PP} = 13.7 Hz, 1P), –6.96 (d, *J*_{PP} = 14.8 Hz, 3P). Anal. Calcd for C₆₃H₅₁ClIrN₃P₄ (%): C 62.97, H 4.28, N 3.50; found: C 62.36, H 4.51, N 3.24. HRMS (FAB) calcd for [M]⁺ C₆₃H₅₁ClIrN₃P₄, 1201.2349; found 1201.2345.

[Ir(3)Cl] (10). Tetraphosphine **3** (200 mg, 0.21 mmol) and [Ir(cod)Cl]₂ (70 mg, 0.10 mmol) are stirred in CH₂Cl₂ (8 mL) for 3 days at rt. The resulting orange suspension was concentrated under reduced pressure. Et₂O (20 mL) was added, and the orange solid was collected by filtration and dried in vacuo. Yield: 203 mg (82%). Mp = 272 °C (dec.). ¹H NMR (500 MHz; CD₂Cl₂, 298 K): δ 7.56 (d, *J* = 8.0 Hz, 3H), 7.08 (t, *J* = 7.3 Hz, 3H), 7.05–6.99 (m, 12H), 6.85 (m, 18H), 6.77 (t, *J* = 7.8 Hz, 3H), 6.38 (d, *J* = 8.4 Hz, 3H), 2.62 (d, *J* = 1.4 Hz, 9H). ¹³C NMR (126 MHz; CD₂Cl₂, 298 K): δ 139.3–139.2 (m), 138.3–137.9 (m), 136.8 (d, *J*_{CP} = 9.3 Hz), 129.9 (m), 128.2 (m), 124.2, 122.1, 121.2, 120.9, 116.4, 11.0 (CH₃). ³¹P{¹H}-NMR (202 MHz; CD₂Cl₂, 298 K): δ 53.67 (d, *J*_{PP} = 17.9 Hz, 3P), 6.38 (q, *J*_{PP} = 17.9 Hz, 1P). Anal. Calcd for C₆₃H₅₁ClIrN₃P₄ (%): C 62.97, H 4.28, N 3.50; found: C 61.14, H 4.70, N 3.11. HRMS (FAB) calcd for [M + H]⁺ C₆₃H₅₂ClIrN₃P₄, 1202.2427; found 1202.2412.

[Rh(1)(nbd)]BF₄ (11). Tetraphosphine **1** (200 mg, 0.20 mmol) and [Rh(nbd)₂]BF₄ (77 mg, 0.20 mmol) are stirred in CH₂Cl₂ (10 mL) for 1 h at rt. The resulting orange-red solution was concentrated under reduced pressure, and hexanes (10 mL) were added to precipitate an orange-red solid. The solid was collected by filtration and washed with hexanes (10 mL). Yield: 260 mg (99%). ¹H NMR (500 MHz; CD₂Cl₂; 298 K): δ 7.57 (d, *J* = 7.9 Hz, 3H), 7.39 (t, *J* = 7.7 Hz, 3H), 7.34 (t, *J* = 7.9 Hz, 6H), 7.20 (t, *J* = 7.6 Hz, 6H), 7.14 (t, *J* = 7.6 Hz, 9H), 7.08 (t, *J* = 7.5 Hz, 6H), 6.81 (s, 6H), 6.58 (d, *J* = 8.4 Hz, 3H), 6.34–6.32 (m, 1H), 6.26–6.25 (m, 1H), 5.37 (s, 1H), 4.55 (s, 1H), 2.76 (s, 1H), 2.38 (s, 1H), 1.28 (s, 9H), 1.05 (d, *J* = 7.6 Hz, 1H), 1.00 (d, *J* = 7.6 Hz, 1H) ppm. ¹³C NMR (126 MHz; CD₂Cl₂, 298 K): δ 139.8, 136.5, 132.5 (m), 130.6 (m), 130.5, 130.1, 129.5 (m), 129.1 (m), 127.5, 127.4, 127.2, 123.7, 121.7, 113.5, 49.3, 48.5, 9.61 (CH₃) ppm. ³¹P{¹H}-NMR (202 MHz; CD₂Cl₂; 298 K): δ 132.36 (dq, *J*_{RhP} = 137.8 Hz, *J*_{PP} = 36.7 Hz, 1P), 6.43 (dd, *J*_{RhP} = 129.5 Hz, *J*_{PP} = 36.3 Hz, 3P) ppm. Anal. Calcd for the CH₂Cl₂ adduct C₇₁H₆₁BCl₂F₄N₃P₄Rh (%): C 63.60, H 4.59, N 3.13; found: C 64.00, H 4.98, N 3.00. HRMS (FAB) calcd for [M – nbd – BF₄]⁺ C₆₃H₅₁N₃P₄Rh, 1076.2089; found 1076.2081.

[Rh(1)(CO)]BF₄ (12). In a stainless steel autoclave, a solution of complex **11** (100 mg, 0.08 mmol) in CH₂Cl₂ (3 mL) was stirred overnight under 25 bar CO at rt. The resulting orange solution was concentrated in vacuo, and the residue was washed with hexanes (2 × 5 mL) to give a light orange powder. Crystals suitable for X-ray single crystal diffraction were obtained by slow diffusion of hexane in a CH₂Cl₂ solution at rt. Yield: 49 mg (51%). FT-IR: ν_{CO} = 2000 cm⁻¹. ¹H NMR (500 MHz; CD₂Cl₂; 298 K): δ 7.58 (d, *J* = 8.0 Hz, 3H), 7.46 (t, *J* = 7.3 Hz, 3H), 7.35 (t, *J* = 7.6 Hz, 3H), 7.28 (t, *J* = 7.5 Hz, 6H), 7.22–7.15 (m, 12H), 6.95–6.87 (m, 12H), 6.73 (d, *J* = 8.4 Hz, 3H), 1.60 (s, 9H)

ppm. ^{13}C NMR (126 MHz; CD_2Cl_2 ; 298 K): δ 139.7 (m), 136.7 (m), 135.2–134.7 (m), 133.8–133.5 (m), 133.2 (m), 131.4, 130.6 (m), 130.2, 129.4 (m), 129.2 (m), 128.6 (d, $J_{\text{CP}} = 14.9$ Hz), 127.5, 124.2, 121.9, 113.8, 10.2 (CH_3) ppm. $^{31}\text{P}\{^1\text{H}\}$ -NMR (202 MHz; CD_2Cl_2 ; 298 K): δ 129.63 (dq, $J_{\text{RhP}} = 115.0$ Hz, $J_{\text{PP}} = 38.8$ Hz, 1P), 16.26 (dd, $J = 126.3$ Hz, $J_{\text{PP}} = 39.1$ Hz, 3P) ppm. Anal. Calcd for $\text{C}_{64}\text{H}_{51}\text{BF}_4\text{N}_3\text{O}_4\text{Rh}$ (%): C 64.50, H 4.31, N 3.53; found: C 63.24, H 4.77, N 3.14. HRMS (FAB) calcd for $[\text{M} - \text{BF}_4]^+$ $\text{C}_{64}\text{H}_{51}\text{N}_3\text{O}_4\text{Rh}$, 1104.2038; found 1104.2043.

[Rh(1)(H)Cl]PF₆ (13)(PF₆). Complex [7]PF₆ (19 mg, 0.02 mmol) was charged to a 5 mm high-pressure NMR-tube and dissolved in CD_2Cl_2 . The tube was put under 5 bar of H_2 , and the reaction followed by NMR spectroscopy. Quantitative conversion to complex **13** was observed after 6 days. Unambiguous characterization of this compound as [Rh^{III}(1)(H)Cl]PF₆ was established by comparison with an authentic sample (vide infra, different anion). [Rh(1)(H)Cl]OTf ((13)(OTf)) was prepared by reaction of **7** (150 mg, 0.14 mmol) with 1 equiv of HOTf (22 mg, 0.15 mmol) in CH_2Cl_2 (8 mL) for 1 h. The solvent was evaporated in vacuo, and the residue was washed with pentanes. After drying in vacuo, a dark-purple solid was obtained. Yield: 151 mg (89%). ^1H NMR (500 MHz; CD_2Cl_2 ; 298 K): δ 7.84 (d, $J = 7.9$ Hz, 1H), 7.67–7.55 (m, 6H), 7.54–7.22 (m, 18H), 7.20–7.16 (m, 2H), 7.12 (td, $J = 7.8, 2.7$ Hz, 2H), 7.04 (t, $J = 7.2$ Hz, 1H), 6.91 (d, $J = 8.5$ Hz, 1H), 6.73–6.63 (m, 6H), 6.53 (dd, $J = 11.5, 8.0$ Hz, 2H), 6.37 (d, $J = 8.5$ Hz, 1H), 6.23 (d, $J = 8.4$ Hz, 1H), 5.97 (br s, 1H), 2.03 (s, 3H), 1.70 (s, 3H), 1.61 (s, 3H), –6.49 (ddt, $J_{\text{HPtrans}} = 167.6$ Hz, $J_{\text{HPcis}} = 19.1$ Hz, $J_{\text{HRh}} = 9.6$ Hz, 1H) ppm. ^{13}C NMR (126 MHz; CD_2Cl_2 ; 298 K): δ 140.5 (d, $J_{\text{CP}} = 5.4$ Hz, C_q), 140.4 (d, $J_{\text{CP}} = 5.0$ Hz, C_q), 139.82 (d, $J_{\text{CP}} = 4.7$ Hz, C_q), 139.76 (d, $J_{\text{CP}} = 4.9$ Hz, C_q), 139.3 (m, C_q), 137.40 (d, $J_{\text{CP}} = 3.8$ Hz, C_q), 137.35 (d, $J_{\text{CP}} = 3.5$ Hz, C_q), 136.7 (d, $J_{\text{CP}} = 3.3$ Hz, C_q), 136.6 (d, $J = 3.8$ Hz, C_q), 135.6, 135.5, 135.21 (d, $J_{\text{CP}} = 4.4$ Hz, C_q), 135.15 (d, $J_{\text{CP}} = 4.3$ Hz, C_q), 135.0 (m, C_q), 134.8 (C_q), 134.5 (C_q), 134.3 (C_q), 134.0 (C_q), 133.6, 133.5, 133.1 (d, $J_{\text{CP}} = 2.1$ Hz), 133.0 (d, $J_{\text{CP}} = 2.1$ Hz), 132.7 (C_q), 132.5 (d, $J_{\text{CP}} = 2.7$ Hz), 132.3 (C_q), 132.2 (C_q), 131.9 (d, $J_{\text{CP}} = 2.3$ Hz), 131.8 (d, $J_{\text{CP}} = 3.1$ Hz), 131.7, 131.6, 131.31 (d, $J_{\text{CP}} = 2.4$ Hz), 131.24, 131.16 (d, $J_{\text{CP}} = 1.3$ Hz), 130.9, 130.8, 130.5 (d, $J_{\text{CP}} = 2.4$ Hz), 130.3 (C_q), 130.0 (C_q), 129.7, 129.6, 129.5, 129.4, 129.3, 129.2 (d, $J_{\text{CP}} = 3.1$ Hz), 128.9, 128.8, 128.0 (d, $J_{\text{CP}} = 4.1$ Hz), 127.9, 125.9 (C_q), 125.8, 125.6 (C_q), 125.5, 125.4 (m, C_q), 124.9, 124.5, 124.1 (m, C_q), 124.0 (d, $J_{\text{CP}} = 9.4$ Hz, C_q), 123.7 (d, $J_{\text{CP}} = 9.1$ Hz, C_q), 122.5, 122.3, 122.1, 116.1, 114.0 (d, $J_{\text{CP}} = 3.0$ Hz), 12.0 (CH_3), 11.9 (CH_3), 10.6 (CH_3) ppm. $^{31}\text{P}\{^1\text{H}\}$ -NMR (202 MHz; CD_2Cl_2 ; 298 K): δ 115.71 (m, 1P), 20.63 (dddd, $J_{\text{PPtrans}} = 371.3$ Hz, $J_{\text{PRh}} = 88.1$ Hz, $J_{\text{PPcis}} = 26.6$ Hz, $J_{\text{PPcis}} = 17.8$ Hz, 1P), 15.00 (ddt, $J_{\text{PPtrans}} = 371.2$ Hz, $J_{\text{PRh}} = 97.3$ Hz, $J_{\text{PPcis}} = 17.2$ Hz, 1P), –1.69 (m, 1P) ppm. The J_{PP} and J_{RhP} coupling constants are disturbed by the J_{HP} coupling from the hydride, which is not entirely decoupled.

Cu^I-Catalyzed Cyclopropanation. AgOTf (1.3 mg, 0.005 mmol) and the corresponding copper complex (0.005 mmol) were stirred at rt in dry CH_2Cl_2 (5 mL) for 10 min. To this mixture, styrene (0.458 mL, 4.0 mmol) and EDA (0.053 mL, 0.5 mmol) were added, and the reaction mixture was stirred for 18 h at rt. Evaporation of the solvent gave the crude product, which was analyzed by ^1H NMR to determine conversion and selectivity.

EPR Spectroscopy. Experimental X-band EPR spectra were recorded on a Bruker EMX spectrometer equipped with a He temperature control cryostat system (Oxford Instruments). The spectra were simulated by iteration of the anisotropic g values, (super)hyperfine coupling constants and line widths.

DFT Geometry Optimizations and Spectral Parameter Calculations. The geometry optimizations were carried out with the Turbomole program^{44a} coupled to the PQS Baker optimizer.⁴⁵ Geometries were fully optimized as minima at the BP86⁴⁶ level using the Turbomole SV(P) basis set^{44c,d} on all atoms. EPR parameters⁴⁷ were calculated with the ADF⁴⁸ program system using the BP86⁴⁶ functional with the ZORA/TZP basis set supplied with the program (all electron, core double- ζ , valence triple- ζ polarized basis set on all atoms), using the coordinates from the structures optimized in Turbomole as input. Orbital and spin density plots were generated with Molden.⁴⁹ Calculated UV–vis spectra based on TD-DFT calculations were obtained with Orca⁵⁰ at the ri-DFT, BP86, SV(P)-SV/J level, using the Tamm-Dancoff approximation (TDA) and COSMO (CH_2Cl_2) solvent corrections.

X-ray crystallography. All data and details are compiled in the Supporting Information.

Acknowledgment. This research was supported by the National Research School Combination on Catalysis (NRSC-C), the University of Amsterdam and the Marie-Curie International Training Network (R)EvCAT funded by the EU. J.I.v.d.V. is grateful to the Dutch Research Council—Chemical Sciences (NWO—CW) for a VENI Innovative Research grant. We thank J. W. H. Peeters for measuring high resolution mass spectra, Dr. D. G. H. Hetterscheld for help with NMR spectroscopy, T. Mahabiersing and W.I. Dzik for assistance with cyclic voltammetry measurements, Dr. Martin Lutz (Univ. Utrecht) for solving the molecular structure of complex **6** by X-ray crystallography, and Prof. F. Neese (Univ. Bonn, Germany) for a copy of his EPR simulation program.

Supporting Information Available: NMR spectra of complex **13**, molecular structures of ligands **1** and **3** and complex **7**, experimental details for reactivity of **7** toward acids, UV–vis spectra and TD-DFT simulations of **7** and [7]PF₆, X-ray crystallographic details and crystallographic information files (CIF). This material is available free of charge via the Internet at <http://pubs.acs.org>.

(44) (a) Ahlrichs, R.; Bär, M.; Baron, H.-P.; Bauernschmitt, R.; Böcker, S.; Ehrig, M.; Eichkorn, K.; Elliott, S.; Furche, F.; Haase, F.; Häser, M.; Hättig, C.; Horn, H.; Huber, C.; Huniar, U.; Kattannek, M.; Köhn, A.; Kölmel, C.; Kollwitz, M.; May, K.; Ochsenfeld, C.; Öhm, H.; Schäfer, A.; Schneider, U.; Treutler, O.; Tsereteli, K.; Unterreiner, B.; von Arnim, M.; Weigend, F.; Weis, P.; Weiss, H. *Turbomole*, Version 5; Theoretical Chemistry Group, University of Karlsruhe: Karlsruhe, Germany, 2002. (b) Treutler, O.; Ahlrichs, R. *J. Chem. Phys.* **1995**, *102*, 346. (c) Turbomole basis set library, Turbomole Version 5, see: (d) Schäfer, A.; Horn, H.; Ahlrichs, R. *J. Chem. Phys.* **1992**, *97*, 2571. (e) Andrae, D.; Hauessermann, U.; Dölg, M.; Stoll, H.; Preuss, H. *Theor. Chim. Acta* **1990**, *77*, 123. (f) Schäfer, A.; Huber, C.; Ahlrichs, R. *J. Chem. Phys.* **1994**, *100*, 5829.

(45) (a) PQS, version 2.4; Parallel Quantum Solutions: Fayetteville, AK, 2001 (the Baker optimizer is available separately from PQS upon request); (b) Baker, J. *J. Comput. Chem.* **1986**, *7*, 385.

(46) (a) Becke, A. D. *Phys. Rev. A* **1988**, *38*, 3098–3100. (b) Perdew, J. P. *Phys. Rev. B* **1986**, *33*, 8822–8824.

(47) Some references and reviews on DFT approaches to EPR parameters: (a) van Lenthe, E.; van der Avoird, A.; Wormer, P. E. S. *J. Chem. Phys.* **1997**, *107*, 2488. (b) van Lenthe, E.; van der Avoird, A.; Wormer, P. E. S. *J. Chem. Phys.* **1998**, *108*, 4783. (c) Neese, F. *Curr. Opin. Chem. Biol.* **2003**, *7*, 125. (d) Neese, F.; Solomon, E. In *Magnetoscience - From Molecules to Materials*; Miller, J. S., Drillon, M., Eds.; Wiley: New York, 2003; pp 345–466; (e) Peng, G.; Nichols, J.; McCullough, E. A.; Spence, J. *Inorg. Chem.* **1994**, *33*, 2857–2864.

(48) (a) Baerends, E. J.; Ellis, D. E.; Ros, P. *Chem. Phys.* **1973**, *2*, 41. (b) Versluis, L.; Ziegler, T. *J. Chem. Phys.* **1988**, *88*, 322. (c) te Velde, G.; Baerends, E. J. *J. Comput. Phys.* **1992**, *99*, 84. (d) Fonseca Guerra, C.; Snijders, J. G.; te Velde, G.; Baerends, E. J. *Theor. Chem. Acc.* **1998**, *99*, 391.

(49) Schaftenaar, G.; Noordik, J. H. *J. Comput. Aided Mol. Des.* **2000**, *14*, 123–134.

(50) ORCA—an *ab initio*, density functional and semiempirical program package, Version 2.7.0; Written by Neese, F. with contributions from Becker, U.; Ganyushin, D.; Liakos, D.; Kossmann, S.; Petrenko, T.; Riplinger, C.; Wennmoths, F. Universität Bonn: Bonn, Germany, 2009.